Rapid Pliocene exhumation of the central Greater Caucasus constrained by low-temperature thermochronometry

Boris Avdeev[1] and Nathan A. Niemi[1]

Received 7 October 2010; revised 12 December 2010; accepted 10 January 2011; published 29 March 2011.

[1] Constraining the timing of onset and rates of deformation within the Greater Caucasus mountains is key to understanding their role in accommodating deformation across the Arabia-Eurasia orogen. We present new low-temperature thermochronometric constraints on the Cenozoic thermal evolution of the central Greater Caucasus that elucidate a three-phase cooling history. Between 50 and 30 Ma, cooling within the range was negligible. In Oligocene time, cooling rates throughout the range increased to ~4°C/Myr. These rates remained constant until the early Pliocene time, when they increased again, reaching ~25°C/Myr along the axial part of the range. Rates and timing of Oligocene exhumation are consistent with previous results from the western Greater Caucasus and are proposed to result from onset of subduction of the Greater Caucasus back-arc basin. Rapid exhumation of the Greater Caucasus, beginning in Pliocene time, contrasts with previously reported thermal histories for other portions of the range. Pliocene exhumation of the central Greater Caucasus appears to be tectonically driven and coincides with widespread evidence for a major reorganization of the Arabia-Eurasia plate boundary. We hypothesize that this exhumation, and regionally observed plate reorganization, results from the collision of the Lesser Caucasus with Eurasia, completing the subduction of oceanic lithosphere across this segment of the Arabia-Eurasia plate boundary.

Citation: Avdeev, B., and N. A. Niemi (2011), Rapid Pliocene exhumation of the central Greater Caucasus constrained by low-temperature thermochronometry, *Tectonics*, *30*, TC2009, doi:10.1029/2010TC002808.

1. Introduction

[2] Deformation associated with the Arabia-Eurasia collision zone covers much of southwestern Eurasia (Figure 1), and spans nearly all of Cenozoic time [e.g., *Nikishin et al.*, 2001]. Despite a wealth of stratigraphic, erosional, and structural constraints on the timing of local deformation throughout the orogen, there is no clear consensus on how this localized deformation relates to the onset of Arabia-Eurasia continental collision, with estimates as diverse as Late Cretaceous [*Stocklin*, 1974; *Alavi*, 1994], Eocene [*Hempton*, 1987; *Jassim and Goff*, 2006; *Allen and Armstrong*, 2008], Oligocene–early Miocene [*Yilmaz*, 1993; *Vincent et al.*, 2007; *Robertson*, 2000; *Fakhari et al.*, 2008], middle Miocene [*Dewey et al.*, 1986; *Şengör and Kidd*, 1979; *McQuarrie et al.*, 2003], and late Miocene–early Pliocene [*Zonenshain and Le Pichon*, 1986; *Philip et al.*, 1989; *Khain*, 1994] having been proposed. In part, this uncertainty results from the spatial and temporal complexities in the evolution of the collision zone. The Arabia-Eurasia collision is not composed of a single suture, but is a mosaic of island arcs and microcontinents whose assembly along the complex paleogeographic margin of Neotethys [e.g., *Golonka*, 2004] is marked by numerous collisional events. Furthermore, final continent-continent collision is still incomplete along the Caspian segment of the collision zone, where oceanic, or thinned continental, crust of the south Caspian Basin continues to subduct northward under the northern Caspian Sea [*Jackson et al.*, 2002].

[3] Reorganization of the Arabia-Eurasia plate boundary at ~5 Ma is both more widely accepted and more accurately temporally constrained than estimates of the onset of Arabia-Eurasia collision [*Wells*, 1969; *Westaway*, 1994; *Axen et al.*, 2001; *Allen et al.*, 2004; *Copley and Jackson*, 2006]. Evidence for plate boundary reorganization includes rapid exhumation of the Alborz [*Axen et al.*, 2001], comparison of fault slip rates with total offsets, which suggests Pliocene initiation of many active faults [*Allen et al.*, 2004; *Copley and Jackson*, 2006], initiation of the North and East Anatolian faults [*Şengör and Kidd*, 1979; *Arpat and Şaroğlu*, 1972], and rapid subsidence in the South Caspian basin [e.g., *Allen et al.*, 2002]. The driving forces of this plate reorganization, however, remain controversial. Based on the assumption of a late Eocene Arabia-Eurasia collision, *Wells* [1969] proposed that the opening of the Red Sea could be such a driving force. Alternatively, *Allen et al.* [2004] argued for the gravitationally driven shifting of deformation away from overthickened Turkish-Iranian plateau and Greater Caucasus crust into topographically lower foreland

[1]Department of Geological Sciences, University of Michigan, Ann Arbor, Michigan, USA.

0278-7407/11/2010TC002808

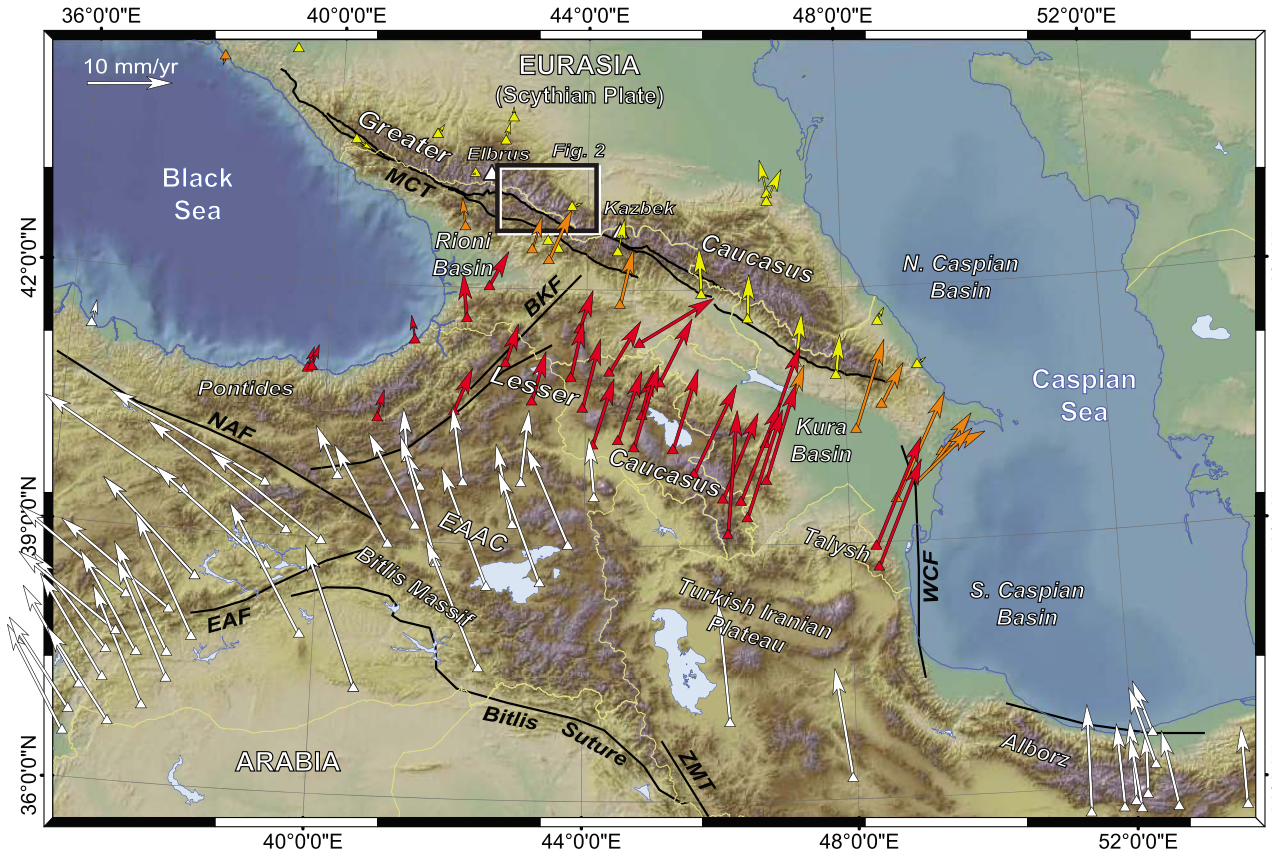

Figure 1. Shaded relief DEM of the Arabia-Eurasia orogen with the major tectonic elements labeled. NAF, North Anatolian Fault; EAF, East Anatolian Fault; EAAC, East Anatolian Accretionary Complex; BKF, Borjomi-Kazbek Fault; MCT, Main Caucasus Thrust; ZMT, Zagros Main Thrust; WCF, West Caspian Fault. Vectors show GPS velocities relative to Eurasia [*Reilinger et al.*, 2006; *Kadirov et al.*, 2008] color coded by region (yellow, Greater Caucasus; orange, Rioni and Kura basins; red, Lesser Caucasus; white, other regions). Box between Mount Elbrus and Mount Kazbek shows the area depicted in Figure 2.

areas. *Copley and Jackson* [2006], based on new data on the crustal thickness of the Turkish-Iranian plateau, argued for mantle driven dynamic uplift of the plateau, rather than crustal thickening, and a resulting shift in deformation loci. On the other hand, if the onset of continent-continent collision is late Miocene [e.g., *Zonenshain and Le Pichon*, 1986], no other forcing beyond the collision itself is needed to drive this plate reorganization.

[4] The complex nature of continental assembly and collision along the Arabia-Eurasia margin, the evidence for recent plate boundary reorganization, and the presence of ongoing subduction within the collision zone makes the Arabia-Eurasia orogenic system a natural laboratory for study of the early stages of continental collision that could provide insight into the evolution of more mature orogens and a better understanding of the spatial and temporal patterns of lithospheric deformation during the process of continental collision. Within this natural laboratory, the Greater Caucasus are particularly well situated to address these problems. The Greater Caucasus are the northernmost tectonic element of the Arabia-Eurasia collision zone (Figure 1) and the highest mountain range in Europe. The Greater Caucasus are a locus of ongoing continental shortening [*Reilinger et al.*, 2006], but lie adjacent to the Caspian zone of intraorogenic subduction [*Jackson et al.*, 2002]. Despite their topographic prominence in the Arabia-Eurasia orogenic system, the role of the Greater Caucasus in accommodating strain throughout the evolution of the orogen is poorly understood. This stems from controversies surrounding both the timing of closure of Neotethys and the beginning of continental collision along the Arabian-Eurasian margin, as well as uncertainty regarding the onset of uplift and exhumation of the Greater Caucasus themselves.

[5] Eocene to Oligocene deformation in the Greater Caucasus is documented by olistostromes and a regional angular unconformity at the base of the Oligocene–early Miocene Maikop formation [*Milanovsky and Khain*, 1963; *Robinson et al.*, 1996; *Banks et al.*, 1997; *Kopp*, 2007; *Leonov*, 2007; *Vincent et al.*, 2007] that has been interpreted as a far-field response to the initiation of continental collision [*Vincent et al.*, 2007; *Allen and Armstrong*, 2008]. Whether or not this deformation led to significant crustal thickening and exhumation in the Paleogene, however, remains unclear [e.g., *Cloetingh et al.*, 2007]. Other authors [e.g., *Zonenshain and Le Pichon*, 1986; *Philip et al.*, 1989; *Khain*, 1994; *Ershov et al.*, 2003; *Morton et al.*, 2003] have suggested late Miocene onset of deformation and uplift. Their conclusions are supported by the widespread occurrence of late Miocene conglomerates, the influx of Greater

Caucasus derived clastics into surrounding sedimentary basins and the rapid subsidence of the northern Caucasus basin.

[6] Links between deformation within the Greater Caucasus and Pliocene plate reorganization are equally poorly constrained. Based on evidence of late Eocene deformation in the Greater Caucasus, *Allen et al.* [2004] suggested that increased gravitational potential across the range, resulting from shortening and crustal thickening, was a driving force of plate boundary reorganization in Miocene-Pliocene time. On the other hand, estimates of late Miocene or Pliocene exhumation and uplift of the Greater Caucasus [*Zonenshain and Le Pichon*, 1986; *Khain*, 1994] would suggest that the evolution of the Greater Caucasus is a response to plate boundary reorganization and not a driving force of it. Improved constraints on the timing of crustal deformation within the range are one approach to distinguish between these scenarios, and to better understand the role of the Greater Caucasus in accommodating strain throughout the evolution of the Arabia-Eurasia plate boundary.

[7] Low-temperature thermochronometry provides a tool to constrain the timing and rates of exhumation in compressional orogens [e.g., *Reiners et al.*, 2003; *Blythe et al.*, 2007; *Clark and Bilham*, 2008]. To the extent that the surface processes responsible for exhumation in compressional orogens are coupled to tectonic forcing [e.g., *Whipple and Tucker*, 1999], low-temperature thermochronometers provide a constraint on the timing and rate at which surface topography develops [e.g., *Braun*, 2005]. Such data has elucidated the timing of crustal exhumation and its relationship to the regional tectonic evolution of northern Iran [e.g., *Axen et al.*, 2001; *Guest et al.*, 2006], but has seen little application to the remainder of the Arabia-Eurasia collision zone [e.g., *Boztuğ and Jonckheere*, 2007; *Okay et al.*, 2010]. To our knowledge, only two regional low-temperature thermochronometry studies of the Greater Caucasus have been completed. One, using apatite fission track methods [*Kral and Gurbanov*, 1996], yielded a variety of cooling ages from the central portion of the Greater Caucasus, ranging from Paleogene to Pliocene, from which the most robust conclusion that can be drawn is that at least some portions of the Greater Caucasus have undergone significant post-Miocene exhumation. Another study, concentrated on the western end of the Greater Caucasus [*Vincent et al.*, 2010], reveals slow post-Eocene exhumation of modest magnitude (less than 5 km).

[8] Here we present the results of a new low-temperature thermochronometric study of the central Greater Caucasus, between Mount Elbrus and Mount Kazbek (Figure 1). This region is ideal for applying low-temperature thermochronometric techniques to studying strain accommodation within the Greater Caucasus. First, there are large exposures of silicic igneous and metamorphic rocks that yield the mineral phases necessary for low-temperature thermochronometry (Figure 2). Second, high-relief valleys, eroded by both fluvial and glacial processes, afford the opportunity to collect vertical transects in excess of 1 km. Finally, modern geodetic observations suggest that at this longitude strain north of the Turkish-Iranian plateau is accommodated almost exclusively within the Greater Caucasus, along a single thrust zone bounding the southern margin of the range. This differs from regions further to the east where strain accommodation is distributed across both the Lesser and the Greater Caucasus, and on both south and north verging thrust systems bounding both sides of the Greater Caucasus range (Figures 1 and 3).

2. Low-Temperature Thermochronometry

[9] We present new apatite (U-Th)/He, apatite fission track, zircon (U-Th)/He, zircon fission track, and K-feldspar $^{40}Ar/^{39}Ar$ ages for the central Greater Caucasus, alongside existing apatite fission track ages [*Kral and Gurbanov*, 1996], to derive the long-term spatial and temporal patterns of exhumation of the range. These low-temperature thermochronometers have closure temperatures of ~70°C (apatite (U-Th)/He [*Wolf et al.*, 1996]), ~110°C (AFT) [*Gleadow et al.*, 1983], ~180°C (zircon (U-Th)/He [*Reiners et al.*, 2003]), ~240°C ($^{40}Ar/^{39}Ar$ [*Foland*, 1994]), and ~232°C–~342°C (ZFT) [*Tagami et al.*, 1998], although these estimates vary with grain size, cooling rate and radiation damage [e.g., *Farley and Stockli*, 2002; *Dodson*, 1973; *Shuster et al.*, 2006; *Flowers et al.*, 2009]. This suite of thermochronometers samples cooling related to exhumation through the upper ~10 km of the crust, depending upon the geothermal gradient, and is most relevant to understanding the recent thermal evolution of the range.

[10] Samples were collected from igneous and metamorphic rocks, primarily granitoids and granite gneisses, likely to yield sufficient quantities of apatite and zircon for analysis. Elevation transects [e.g., *Wagner and Reimer*, 1972; *Gallagher et al.*, 2005] were collected where significant topographic relief was present within a single igneous or metamorphic unit. Structural complexities within the Greater Caucasus basement rocks and poor constraints on sample paleodepth limited the application of this sampling strategy elsewhere within the range. Instead, multiple low-temperature thermochronometers were analyzed for individual samples to derive a continuous cooling path [e.g., *McAleer et al.*, 2009]. As discussed below, not all samples yielded a complete suite of reset cooling ages, and some higher-temperature thermochronometric results are consistent with the presumed age of igneous crystallization or peak metamorphism. These results are obviously not reflective of the Cenozoic evolution of the Greater Caucasus, but do provide constraints on the maximum amount of exhumation that these rocks could have experienced during the Cenozoic.

2.1. Analytical Methods

[11] All samples were collected after removal of the outer few centimeters of rock to prevent inclusion of material affected by forest fires or lightning [*Mitchell and Reiners*, 2003]. Rocks were crushed and pulverized, and mineral concentrates were made using standard magnetic and density techniques. Individual mineral grains of apatite and zircon were handpicked from the concentrates, with care taken to avoid comminuted grains or grains with inclusions visible under 200× magnification.

[12] Apatite (U-Th)/He analyses were conducted on single-apatite grains at the Caltech Noble Gas Laboratory using standard procedures [*Farley and Stockli*, 2002]. Sample aliquots were outgassed using a Nd-YAG laser [*House et al.*, 2000] and ^{4}He was measured by ^{3}He spike

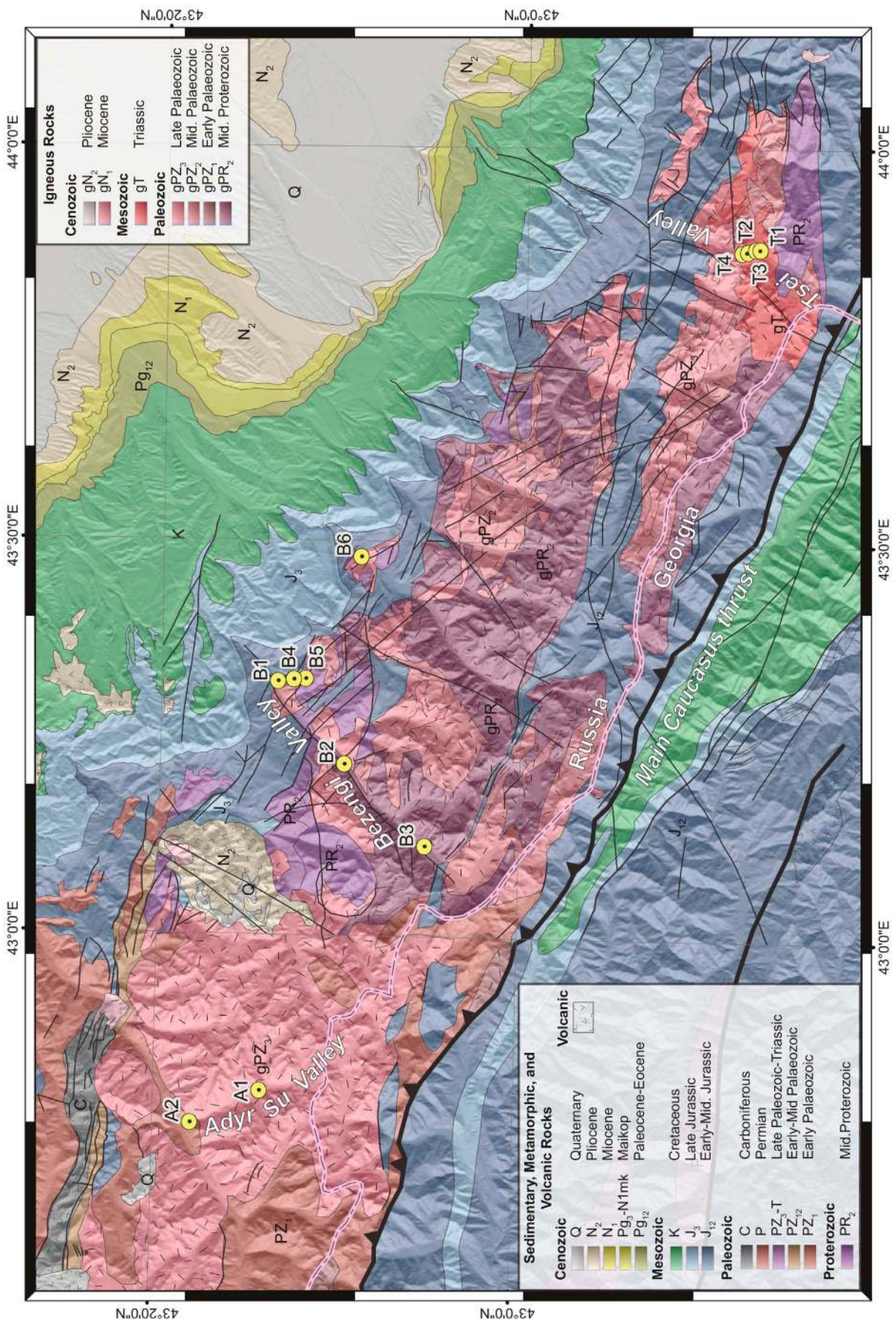

Figure 2. Map of the central Greater Caucasus with locations of low-temperature thermochronometry samples shown as yellow dots. Geology modified after *Pismennyj* [2002], *Gamkrelidze and Kakhadze* [1959], and *Nalivkin* [1976].

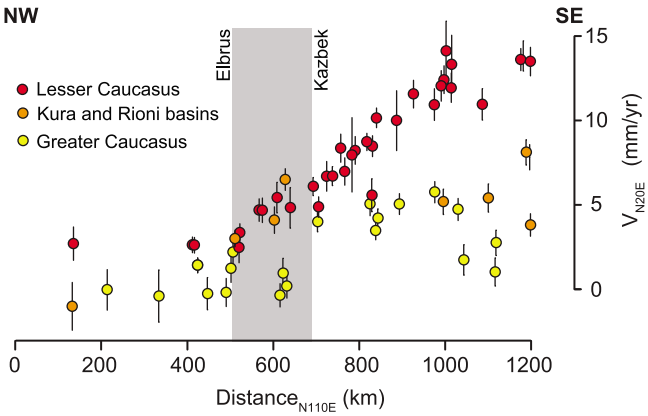

Figure 3. Caucasus region GPS velocities [*Reilinger et al.*, 2006; *Kadirov et al.*, 2008]. Velocities in the N20E (plate-convergence-parallel) direction are shown plotted against orogen-strike-parallel distance (N110E). Color coding of GPS velocities as in Figure 1. Present-day strain distribution varies along strike of the Caucasus. West of Mount Elbrus, little or no strain is accommodated across the Caucasus (GPS velocities are within error of stable Eurasia). Between Mount Elbrus and Mount Kazbek, strain is localized on the Main Caucasus Thrust (Greater Caucasus velocities are within error of stable Eurasia; Lesser Caucasus and Kura/Rioni basin velocities are indistinguishable at 3–5 mm/yr with respect to Eurasia). East of Mount Kazbek, strain is broadly distributed, with Greater Caucasus sites moving several millimeters per year with respect to stable Eurasia, likely due to shortening in the north verging fold-and-thrust belt in Dagestan, and considerable shortening between the Lesser Caucasus and both the Kura Basin and the Greater Caucasus.

using a quadrupole mass spectrometer. ^{238}U, ^{235}U, ^{232}Th and ^{147}Sm were measured using isotope dilution ICP mass spectrometry [*Farley and Stockli*, 2002]. Reproducibility of analytical results was constrained by 4–6 replicate analyses. Analytical uncertainty of apatite (U-Th)/He ages is ~5% (1σ) based on instrument precision and error in the alpha ejection correction [*Farley et al.*, 1996]. The Durango fluorapatite standard ((U-Th)/He age of 31.4 Ma [*McDowell et al.*, 2005]) was analyzed in all sample runs to check age accuracy. The reported error for each sample is the standard deviation of the replicate analyses, which typically exceeded the analytical uncertainty, as has previously been observed for geologic samples [e.g., *Farley and Stockli*, 2002]. Two outliers were excluded from the data set after failing the Q-test [*Dean and Dixon*, 1951] at the 95% level of confidence (Tables 1 and A1). Undetected microinclusions of U- and Th-bearing phases within the apatite are the most likely explanation for the outlier ages.

[13] Apatite and zircon fission track ages were determined by Apatite to Zircon, Inc. [*Donelick et al.*, 2005]. Polished apatite grain mounts were immersed in 5.5N HNO_3 for 20 s at 21°C to reveal natural fission tracks. Zircon grain mounts were immersed in an eutectic melt of NaOH + KOH at ~210°C (±10°C) for ~34 h. Track densities were counted and recorded. Concentrations of radiogenic elements were determined for the localities of counted natural fission tracks by measuring ^{238}U, ^{232}Th and ^{147}Sm via LA-ICP-MS [*Hasebe et al.*, 2004]. Apatite grain mounts were then irradiated with ~10^7 tracks/cm^2 from a ^{252}Cf source. Irradiated grain mounts were again immersed in 5.5N HNO_3 for 20 s at 21°C to reveal horizontal, confined fission tracks, and track lengths were then measured. Fission track ages were determined using a modified decay equation that includes calibration for the LA-ICP-MS using the Durango fluorapatite standard (fission track age of 30.6 Ma) and Fish Canyon zircon (28.5 Ma).

[14] Zircon (U-Th)/He ages were measured on single-grain aliquots at the Arizona Radiogenic Helium Dating Laboratory following standard protocols [*Reiners et al.*, 2002, 2004]. Euhedral zircons were wrapped in Nb foil and degassed by laser heating. He abundances were measured on a quadrupole mass spectrometer using ^{3}He isotope dilution. Degassed zircons were then dissolved and U and Th concentrations were measured on an ELEMENT 2 ICP-MS. (U-Th)/He ages were corrected for alpha ejection [*Farley*, 2002].

[15] ^{40}Ar/^{39}Ar analysis of potassium feldspars was performed at the University of Michigan Noble Gas Labora-

Table 1. Summary of Low-Temperature Thermochronometry Results

Sample	Longitude (°N)	Latitude (°E)	Altitude (m)	AHe[a] (Ma)	AFT[b] (Ma)	ZHe[c] (Ma)	ZFT[d] (Ma)	^{40}Ar/^{39}Ar[e] (Ma)
A1	42.801008	43.235924	2370		5.2 ± 0.6	24.06 ± 0.49	230.4 ± 13.1	291.2 ± 1.3
A2	42.758738	43.298983	1690		5.1 ± 0.6	88.93 ± 1.81	433.0 ± 19	
B1	43.320785	43.226316	1357	16.81 ± 3.36	21.8 ± 1.1	188.5 ± 3.87	293.4 ± 12.4	250.0 ± 1.2
B2	43.217135	43.163385	1687	4.06 ± 0.4	3.64 ± 0.35			
B3	43.114502	43.087557	2470	12.16 ± 1.11	7.64 ± 0.52			
B4	43.323375	43.211909	1846	11.64 ± 1.75				
B5	43.324428	43.200743	2359	19.03 ± 2.08				
B6	43.480113	43.151325	1052	13.55 ± 2.39				
T1	43.873633	42.785572	2200	2.55 ± 0.45	6.23 ± 0.98	20.4 ± 0.39		
T2	43.873080	42.789768	2421	2.05 ± 0.52				
T3	43.870518	42.797055	2994	1.88 ± 0.63		32.04 ± 0.72		
T4	43.869105	42.802727	3456	1.67 ± 0.21				

[a]Standard error is calculated from replicate analyses. Range of closure temperatures for cooling rates between 1°C/Myr and 25°C/Myr is 52°C–73°C.
[b]Standard error is estimated analytical error. Range of closure temperatures for cooling rates between 1°C/Myr and 25°C/Myr is 98°C–124°C.
[c]Standard error is estimated analytical error. Range of closure temperatures for cooling rates between 1°C/Myr and 25°C/Myr is 162°–192°C.
[d]Standard error is estimated analytical error. Range of closure temperatures predicted by various models (see text) for cooling rates between 1°C/Myr and 25°C/Myr is 210°C–350°C.
[e]Standard error is estimated analytical error. Range of closure temperatures for cooling rates between 1°C/Myr and 25°C/Myr is 221°C–258°C.

tory, following the methods described by *Ownby et al.* [2007]. Samples were wrapped in pure Al foil and irradiated for 20 h at location 5C at the McMaster Nuclear Reactor at McMaster University in Hamilton, Ontario in irradiation package mc19. Standard hornblende MMhb-1 was used as a neutron-fluence monitor with an assumed K-Ar age of 520.4 Ma [*Samson and Alexander*, 1987]. Samples were incrementally heated with a Coherent Innova 5W continuous argon-ion laser until complete fusion was achieved. Ar isotopes were measured using a VG1200S mass spectrometer with a source operating at 150 μA total emission and equipped with a Daly detector operating in analog mode. Fusion system blanks were run every five fusion steps and blank levels from argon masses 36 through 40 ($\sim 2 \times 10^{-14}$, $\sim 4 \times 10^{-14}$, $\sim 1 \times 10^{-14}$, $\sim 2 \times 10^{-14}$, and 2×10^{-12} ccSTP) were subtracted from sample gas fractions. Corrections were also made for the decay of ^{37}Ar and ^{39}Ar, for the production of ^{36}Ar from the decay of ^{36}Cl, as well as interfering nucleogenic reactions from K, Ca and Cl.

2.2. Modeling Methods

[16] Thermal history modeling was undertaken using HeFTy v. 1.6.7 software [*Ketcham*, 2005]. This program implements a variety of forward models for fission track density and annealing in apatite, as well as models of He diffusion in apatite and zircon. Observed apatite fission track densities and c axis projected track length distributions were modeled using a modification of the fanning Arrhenius model [*Ketcham et al.*, 2007, 2009]. Diffusion properties for He in apatite were modeled considering the effects of radiation damage on He diffusion (the RDAAM model [*Flowers et al.*, 2009]). He diffusion in zircon was modeled following *Reiners et al.* [2004]. Thermal models were constrained by modern surface temperatures and, where available, high-temperature constraints from ^{40}Ar/^{39}Ar of feldspars or zircon fission track thermochronometry. No other constraints beyond the annealing or diffusion algorithms described above were imposed. Subsegment spacing of cooling paths was allowed to vary randomly, and monotonic cooling was not assumed. Viable thermal histories were found by simple Monte Carlo inversion. Forward models for randomly generated thermal histories were run until 100 acceptable [*Ketcham*, 2005] models were found.

[17] For ^{40}Ar/^{39}Ar, zircon fission track, and samples on which only apatite (U-Th)/He were analyzed, blocking temperatures [*Dodson*, 1973] were determined assuming a constant cooling rate. We estimated blocking temperatures for a range of cooling rates between 1°C/Myr and 25°C/Myr with the Closure program [*Ehlers et al.*, 2005]. Blocking temperatures for (U-Th)/He data were calculated following *Farley* [2000]. Zircon fission track fanning models [*Tagami et al.*, 1998] and feldspar diffusion models [*Foland*, 1994] were used to estimate the blocking temperatures of zircon FT and ^{40}Ar/^{39}Ar systems. The blocking temperatures of the ZFT and ^{40}Ar/^{39}Ar systems were included, where appropriate, as box constraints in the HeFTy thermal modeling described above.

[18] In cases where a change in cooling rate is observed, a finite element exhumation model (Pecube, SVN version, Rev. 9 [*Braun*, 2003]) was used to calculate the time lag of the thermal signal following the exhumation rate change. The model was computed for a two-step exhumation history with a change of exhumation rate from 0.1 km/Myr to 1 km/Myr. Parameters of the model were set as follows: flat topography, 40 km^2/Myr diffusivity, 0.25°C/Myr heat production at surface, 60 km model thickness and 800°C temperature at the base of the model.

3. Results

[19] Samples were collected from the northern side of the central Greater Caucasus, Russia, between Mount Elbrus and Kazbek along three transects (Figure 2). Two samples analyzed were collected in Adyr Su valley, a tributary of the Baksan river, east of Mount Elbrus. Nine samples were collected near the village of Bezengi, along the Cherek-Balkarskii and Cherek-Bezengskii valleys, located within the Kabardino-Balkaria Nature Preserve (Figure 2). The third transect was collected in Tsei valley, located to the northwest of Kazbek. At Tsei, a complete vertical transect was sampled, while along-valley transects were sampled at Adyr Su and Bezengi.

3.1. Adyr Su

[20] The Adyr Su river drains northward from the Main Caucasus Ridge, which is the border between Russia and Georgia (Figure 2). This river is situated completely within the crystalline core of the range. The higher of the two samples (A1) was collected from a granite of presumed middle to late Paleozoic age [*Gamkrelidze and Kakhadze*, 1959]. A lower sample (A2), was collected down valley, away from the axis of the range. This sample was collected from a K-feldspar-rich granitoid, which is a part of a Precambrian–early Paleozoic metamorphic gneiss complex [*Gamkrelidze and Kakhadze*, 1959].

[21] ^{40}Ar/^{39}Ar ages from sample A1 are Early Permian (~291 Ma), consistent with published crystallization ages of nearby granites [*Gamkrelidze and Kakhadze*, 1959]. Zircon fission track ages from this sample yield a slightly younger Middle Triassic age (~230 Ma), possibly representative of modest exhumation at this time. Sample A2 yields an Early Silurian (~433 Ma) zircon fission track age, consistent with zircon U-Pb ages from orthogneiss in the adjacent Kyrtyk valley [*Somin*, 2007a], and possibly dating gneiss formation.

[22] Lower-temperature thermochronometers from Adyr Su reveal a significantly younger portion of the thermal history. Zircon (U-Th)/He and apatite fission track ages from sample A1 are 24.06 ± 0.49 and 5.2 ± 0.6 Ma, respectively (Table 1). These ages are interpreted as resulting from Cenozoic exhumation associated with uplift and erosion of the Greater Caucasus. Thermal modeling of these data reveals rapid cooling at ~25°C/Myr since ~5 Ma. The rate of cooling prior to 5 Ma is less well resolved, but appears to be negligible cooling, with reheating permissible. Sample A2 yielded zircon (U-Th)/He and apatite fission track ages of 88.93 ± 1.81 and 5.1 ± 0.6 Ma. Differences in zircon (U-Th)/He ages between samples A1 and A2 may reflect differences in paleodepth resulting from structural complexity in the crystalline basement. The Coniacian zircon (U-Th)/He age is consistent with a regional unconformity that developed across the northern Greater Caucasus in Albian-Santonian time [e.g., *Pismennyj*, 2002]. Thermal modeling of the zircon

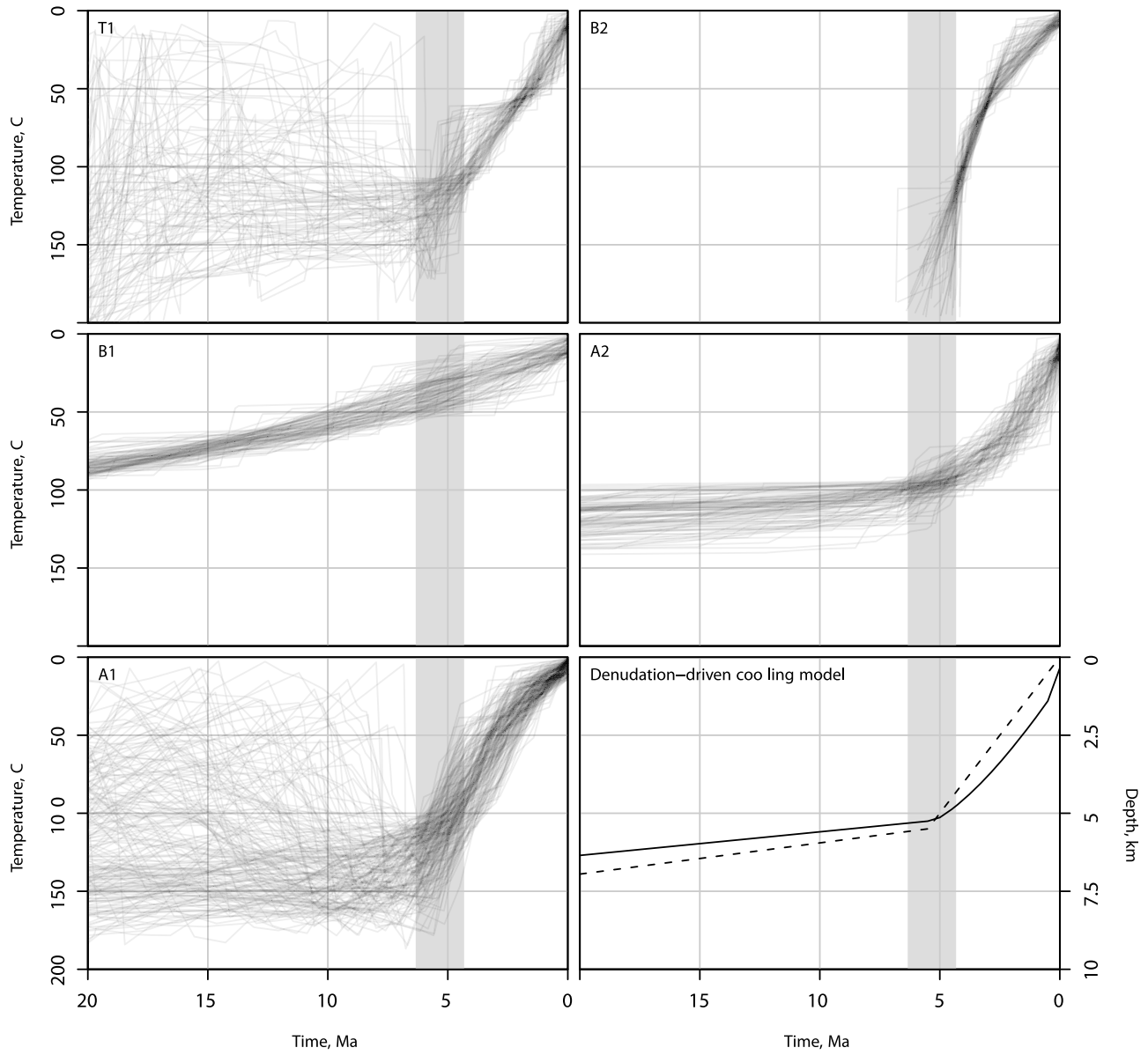

Figure 4. Randomly generated thermal histories satisfying low-temperature thermochronometry data (Tables A1, A2, and A3) for samples that have at least apatite fission track lengths measured. The gray band is centered on Miocene-Pliocene boundary (5.3 Ma). Samples A1, A2, and T1 clearly record the onset of rapid cooling at this time. Sample B1 has cooled past the sensitivity range of the analyzed thermochronometers (<50°C) by 5 Ma, and so it does not record any change in cooling rate at this time. Sample B2, on the other hand, appears to have been hotter than the partial annealing zone of apatite at 5 Ma and thus only records rapid cooling since ~5 Ma. The bottom right panel displays a cooling path (solid line) resulting from an increase in exhumation rate at the Miocene-Pliocene boundary from 0.1 to 1 km/Myr (dashed line shows depth below the surface), predicted from Pecube model [*Braun*, 2003].

(U-Th)/He and apatite fission track data for sample A2 (Figure 4) indicates cooling at a rate of 0.7°C/Myr prior to ~5 Ma, followed by cooling at a rate of 20°C/Myr to the present.

3.2. Bezengi

[23] The Cherek-Bezengi valley lies east of Adyr Su, and crosses almost the whole width of the crystalline core of the Greater Caucasus in a northeast–southwest direction (Figure 2). The Cherek-Bezengi River drains the Bezengi Massif, which overlies the Main Caucasus Thrust, and in which is exposed Proterozoic and Paleozoic metamorphic and igneous rocks. At its northernmost end, the river exposes Early Jurassic and younger Paratethys-related strata, unconformably overlying the older metamorphic infrastructure.

[24] The southernmost sample from Bezengi, B3, was collected from Mesoproterozoic granitoids and yielded a 12.16 ± 1.11 Ma apatite (U-Th)/He age and a 7.64 ± 0.52 Ma

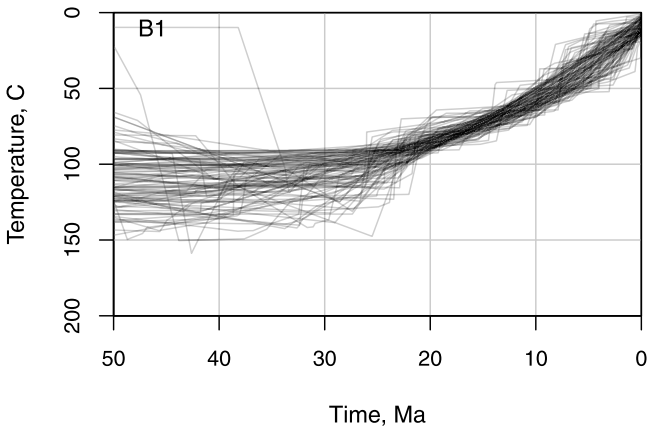

Figure 5. A selection of 100 randomly generated thermal histories satisfying apatite and zircon (U-Th)/He and apatite fission track data (Tables A1, A2, and A3) from the B1 sample in the Bezengi valley, indicating Oligocene change in cooling rate. See text for discussion.

apatite fission track age (Table 1). An explanation for the inverse relationship observed between the thermochronometric ages and commonly cited closure temperatures for this sample is not readily apparent. Recent radiation damage models that predict an increase in apatite (U-Th)/He closure temperature for apatites with high uranium concentrations and slow cooling rates (<0.1°C/Myr [*Shuster et al.*, 2006; *Shuster and Farley*, 2009; *Flowers et al.*, 2009]) offer one possible solution, but U concentrations in sample B3 are not significantly higher than those of other samples in the region (Table A1). Another possible explanation could be eU concentration zoning [*Farley and Stockli*, 2002]. No forward thermal model could be found that adequately fit both the apatite fission track and (U-Th)/He data, however, a rough estimate for cooling rate, averaged over the last 10 Myr is 5°C/Myr to 15°C/Myr.

[25] Sample B2, from a schist near the central portion of the crystalline core, yielded Pliocene apatite fission track and (U-Th)/He ages (3.64 ± 0.35 and 4.06 ± 0.4 Ma; Table 1). Thermal modeling indicates rapid cooling at rates of ~25°C/Myr since at least 4 Ma. No high-temperature thermochronometers, or older fission tracks, constrain the pre-Pliocene thermal evolution of this sample (Figure 4).

[26] The northernmost sample, B1, was collected from Early Carboniferous granite, immediately beneath unconformably overlying Jurassic shallow-marine sedimentary rocks [*Pismennyj*, 2002]. As at Adyr Su, higher-temperature thermochronometers, zircon fission track and potassium feldspar $^{40}Ar/^{39}Ar$, yield Permian to earliest Triassic ages (293.4 ± 12.4 Ma and 250.0 ± 1.2 Ma, respectively; Table 1), consistent with published crystallization ages [*Pismennyj*, 2002]. The zircon (U-Th)/He age (188.5 ± 3.87 Ma; Table 1) of sample B1 records a relatively old thermal event, potentially related to exhumation during Jurassic orogeny, or perhaps simply reflective of long-term slow erosion and cooling.

[27] Low-temperature data from apatite fission track and apatite (U-Th)/He yield ages of 21.8 ± 1.1 and 16.81 ± 3.36 Ma, respectively (Table 1). Thermal modeling of sample B1 indicates slow cooling at a rate of 4°C/Myr during the last ~20 Myr (Figure 4). It should be noted that this sample does not record any changes in cooling rate younger ~16 Ma, the time at which it cooled below the closure temperature for apatite (U-Th)/He. Potential thermal paths for sample B1 between 50 and 20 Ma are poorly constrained, but could not have exceeded 150°C, and are inconsistent with a constant cooling rate from 50 Ma to the present (Figure 5). Three additional apatite (U-Th)/He ages from nearby samples (B4, B5 and B6) yield results similar to those from sample B1 (Table 1), and were not further modeled.

3.3. Tsei

[28] Four samples were collected from a Late Triassic granodiorite [*Pismennyj*, 2002] along the north wall of the Tsei valley, on a 45° transect over a vertical distance of ~1300 m. All thermochronometers from this sample reflect Cenozoic cooling. Zircon (U-Th)/He ages from samples T1 (2200 m) and T3 (2994 m) are 20.4 ± 0.39 Ma and 32.04 ± 0.72 Ma, respectively (Table 1). Given the elevation and age difference between these two samples, the average rate of exhumation from 30 to 20 Ma was ~ 80 m/Myr. If we assume a geothermal gradient of 20°C/km, this is equivalent to a cooling rate of 4°C/Myr during this time period. Apatite (U-Th)/He ages are essentially invariant with elevation across the transect and are ~2 Ma (Table 1), suggesting rapid passage through the closure isotherm (~70°C) at this time. An apatite fission track age of 6.23 ± 0.98 Ma was determined on the lowest sample (T1). Modeling of the thermochronometric data for sample T1 indicates a change in cooling rate from less than 3°C/Myr to 20°C/Myr at ~5 Ma (Figure 4).

4. Discussion

4.1. Amount, Rate and Timing of Exhumation of the Greater Caucasus

[29] The thermochronometric data presented above yield new insights into the amount, timing, and rate of late Cenozoic exhumation of the Greater Caucasus. Higher-temperature thermochronometers, specifically zircon fission track and potassium feldspar $^{40}Ar/^{39}Ar$, throughout the central Greater Caucasus yield late Paleozoic to earliest Mesozoic cooling ages. These ages are consistent with published K-Ar and $^{40}Ar/^{39}Ar$ dates from Paleozoic igneous and metamorphic rocks in the range [*Somin*, 2007b; *Philippot et al.*, 2001], and thus provide an upper bound on the total amount of exhumation of the Greater Caucasus crystalline core. Given the wide range of zircon fission track closure temperature estimates [e.g., *Reiners and Brandon*, 2006], we here use the closure temperature of potassium feldspar (~221°C–258°C for cooling rates of 1°C–25°C) to determine the maximum amount of exhumation. Assuming a geothermal gradient of 20°C/km, no more than ~12 km of exhumation of the Greater Caucasus has occurred since late Paleozoic time (<8 km for a geothermal gradient of 30°C/km). Several samples, however, yielded Cenozoic zircon (U-Th)/He ages, for which the closure temperature range is 162°C–192°C for cooling rates of 1°C/Myr–25°C/Myr. Given a 20°C/km (30°C/km) geothermal gradient, these

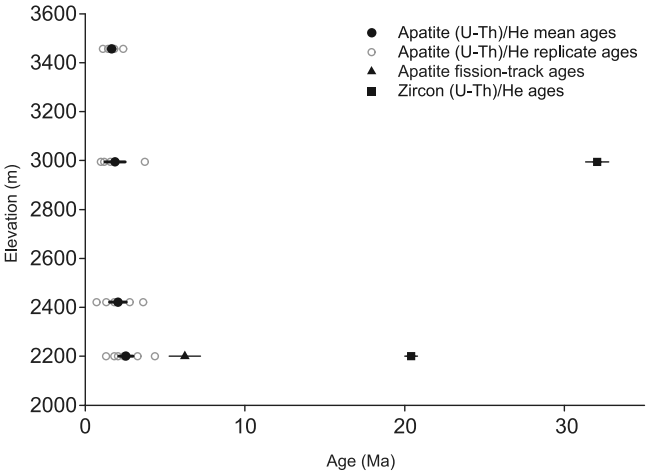

Figure 6. Low-temperature thermochronometric age data from the Tsei valley plotted as a function of sample elevation (samples T1–T4, T1 being the lowermost). Zircon (U-Th)/He reveal slow (~4°C/Myr) cooling between 20 and 30 Ma. Elevation invariant apatite (U-Th)/He ages indicate rapid, but unquantifiable, cooling in the past ~2 Ma. Results of thermal modeling of the lowest-elevation samples are shown in Figure 4.

results require ~9 km (~6 km), or roughly 75%, of the total exhumation of these samples to have occurred since the Oligocene. We have few constraints on the exhumation and/or burial paths taken by these samples throughout the Mesozoic, and do not imply that our results require a simple and monotonic exhumation history. However, depending on the geothermal gradient and cooling rate, 6–12 km of exhumation has occurred in the most deeply exposed portions of the central Greater Caucasus since ~20–30 Ma. Some samples, particularly on the flanks of the range, exhibit significantly less cooling (e.g., sample B1), and may have experienced no more than several kilometers of exhumation in late Cenozoic time. Samples from the northern flank of the range have experienced lesser amounts of exhumation than those to the south, likely reflecting the structural position of the northern samples on the limb of the south vergent anticlinorial structure that defines the range as a whole.

[30] The rate of cooling of the Greater Caucasus is primarily constrained by thermal modeling of samples for which multiple thermochronometers were analyzed (Table 1). Four such samples (Figure 4) reveal rapid exhumation at ~20°C/Myr in post-Miocene time. The vertical transect at Tsei (Figure 6) reveals cooling ages that are statistically invariant with elevation, consistent with rapid, but unquantifiable cooling rates since 2 Ma. Slower rates of cooling prior to 5 Ma are apparent in two multi-thermochronometer samples (Figure 4, samples A2 and B1), which yield cooling rates of ~0°C–4°C/Myr since 20 Ma. Thermal models for two samples, A1 and T1, do not exclude the possibility of rapid cooling and reburial during Miocene time. However, thermal models for samples A2 and B1 do provide constraints that preclude such a complex thermal history. These modeling constraints are consistent with the geologic record, which contains no significant unconformities in Miocene time. A constrained thermal model, imposing a monotonic cooling path for samples A2 and B1, can therefore be imposed (Figure 7). The constrained models for samples A1 and T1 suggest a change in cooling rate from 4°C/Myr to 20°C/Myr at 5 Ma. Zircon (U-Th)/He dates from the vertical transect at Tsei extend pre-Pliocene slow cooling (~4°C/Myr) back to ~30 Ma. Sample B1, from the northern edge of the range, provides a thermal history back to ~50 Ma that requires a rate of cooling slower than ~4°C/Myr prior to ~30 Ma (Figure 5).

[31] No single sample from this data set provides a complete Cenozoic thermal history for the central Greater Caucasus, but, taken as a group, such a history can be constructed. The earliest thermal history of the Greater Caucasus is the least well constrained, but data from sample B1 are consistent with isothermal holding or extremely slow exhumation (<1°C/Myr) between 50 and 30 Ma. At 30 Ma an increase in cooling rate to ~3°C–4°C/Myr is observed in this sample. This is consistent with post-30 Ma cooling rates observed in several other samples (this study and that by *Vincent et al.* [2010]). Rapid cooling at ~20°C/Myr begins at ~5 Ma, and is observed in samples from all three trans-

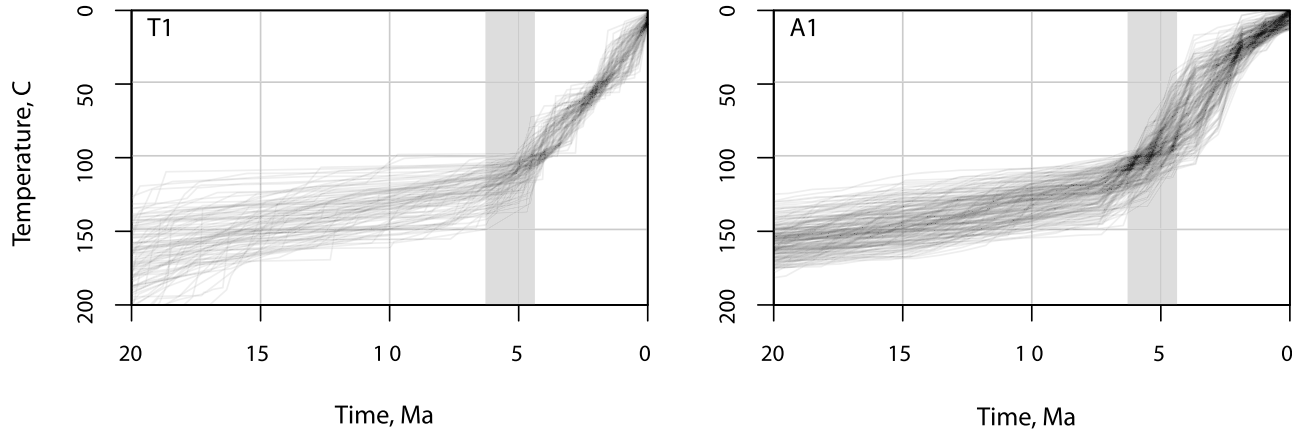

Figure 7. Thermal models for samples A1 and T1 subject to monotonic cooling constraints, as implied by adjacent thermochronometric samples and geologic evidence (see Figure 4 and text for additional discussion).

ects. In addition, young (~2 Ma) apatite (U-Th)/He ages at Tsei imply that rapid cooling in this area has continued to the present at rates exceeding 30°C/Myr. This may reflect, in part, increased glacial erosion of the range in late Pliocene and Pleistocene time.

4.2. Spatial Variations in Exhumation of the Greater Caucasus

[32] Our complete Cenozoic history of the amount, rates, and timing of exhumation of the central Greater Caucasus differ significantly from studies of the western Greater Caucasus [*Vincent et al.*, 2010]. Both studies identify an exhumational event beginning in late Eocene or Oligocene time, and yield similar rates of exhumation, as derived from thermochronometric data, throughout the Oligocene and Miocene. In the western Greater Caucasus, however, the core of the range appears to undergo a reduction in the rate of exhumation in Pliocene and Pleistocene time, limiting the total amount of exhumation to ~2.5 km [*Vincent et al.*, 2010]. Results from the core of the central Greater Caucasus reveal an almost opposite Plio-Pleistocene history, with significant increases in exhumation rates during this time, resulting in substantially greater total amounts of exhumation. Our results, in combination with the data from the western Greater Caucasus [*Vincent et al.*, 2010], appear to confirm suggestions from earlier work [*Kral and Gurbanov*, 1996] that the western and central Greater Caucasus have remarkably different exhumational histories. This variability may be a result of differential shortening along the range due to the westward extrusion of the Anatolia, which may accommodate a significant fraction of the Arabia-Eurasia convergence at the longitude of the western Greater Caucasus. The resulting differential convergence north of the Anatolia is then either diffusely consumed in the western Lesser Caucasus or accommodated by the hypothesized Borjomi-Kazbek strike-slip fault (Figure 1 [*Philip et al.*, 1989]).

4.3. Topographic Growth of the Greater Caucasus

[33] Deriving rates of topographic growth from rates of exhumation is not straightforward [e.g., *England and Molnar*, 1990]. Nonetheless, rates of exhumation across the Greater Caucasus from 30 to 5 Ma are low, ~0.1–0.2 mm/yr (Figure 8), much lower than those typically observed in active orogenic systems [e.g., *Burbank*, 2002]. Cooling rates from thermochronometric sampling in the western Greater Caucasus are of similar magnitude to those reported here [*Vincent et al.*, 2010]. These slow rates, combined with the observation that at least the eastern Greater Caucasus region remained below sea level prior to the late Miocene [*Kopp and Shcherba*, 1985], suggest that the Greater Caucasus did not form a significant topographic barrier during Oligocene or Miocene time. Rapid exhumation of the central Greater Caucasus, at rates consistent with those observed in active orogens [e.g., *Burbank*, 2002] began in late Miocene to early Pliocene time (Figure 8). This change is correlative with the onset of deposition of continental conglomerates on the margins of the Greater Caucasus [e.g., *Khain*, 1994; *Saintot et al.*, 2006] and an increase in sediment derived from the Greater Caucasus [*Morton et al.*, 2003]. Together, these data suggest that the Greater Caucasus became a highstanding orogen no earlier than Pliocene time.

4.4. Relationship of Exhumation in the Greater Caucasus to Regional Tectonics of the Arabia-Eurasia Collision

[34] Given the timing and rates of exhumation described above, it seems pertinent to query the relationship between exhumation of the Greater Caucasus and tectonic and climatic events along the Arabia-Eurasia plate boundary. The earliest observed phase of exhumation, at ~30 Ma, is consistent with stratigraphic and thermochronometric evidence from the western Greater Caucasus suggesting that the range had begun to uplift and was subaerial at this time [*Vincent et al.*, 2007, 2010]. This uplift has been interpreted as a result of the Arabia-Eurasia collision, which several estimates place at the end of Eocene [e.g., *Saintot and Angelier*, 2002; *Allen and Armstrong*, 2008], largely on the basis of deformation in the Greater Caucasus. However, such an explanation is problematic, as combined plate and palinspastic reconstructions require the removal of ~500 km of continental lithosphere (presumably via subduction) from the Eurasian margin to accommodate observed plate convergence if collision initiated at this time [*McQuarrie et al.*, 2003].

[35] Alternatively, it seems reasonable to explain the onset of exhumation in the Greater Caucasus in the late Eocene as a response to the initiation of subduction of the Greater Caucasus back-arc basin [*Zonenshain and Le Pichon*, 1986]. This basin used to lie between Eurasia and the Lesser Caucasus (Figure 1 [*Zonenshain and Le Pichon*, 1986]). No remnants of the basin floor are preserved, but it was likely underlain by oceanic or transitional crust, as are the Black and Caspian seas [e.g., *Knapp et al.*, 2004]. The original width of the Greater Caucasus back-arc basin is poorly constrained, but may have been as great as 900 km [*Zonenshain and Le Pichon*, 1986], potentially accounting for the removed lithosphere required in plate reconstructions of this plate boundary [*McQuarrie et al.*, 2003], if these reconstructions are correct [*Fakhari et al.*, 2009].

[36] Subduction of the Greater Caucasus back-arc basin may have initiated after the late Eocene "soft" collision of Arabia and the Pontide–Lesser Caucasus arc, buffered by the East Anatolian accretionary complex [*Şengör et al.*, 2003, 2008]. The absence of Oligocene or Miocene volcanics on the edge of Eurasia or the northern margin of the Lesser Caucasus may indicate slow and/or flat-slab subduction [*Pindell et al.*, 2005; *Kay and Coira*, 2009], or that the original width of the back-arc basin is substantially less than has been proposed by *Zonenshain and Le Pichon* [1986].

[37] Exhumation rates observed in the Oligocene remain constant across the central Greater Caucasus until Pliocene time, when they increase by a factor of four or more (Figure 8). In many places along the Alpine-Himalayan orogen, Pliocene increases in exhumation rate and sediment supply have been interpreted as resulting from global climate change [*Donnelly*, 1982; *Molnar and England*, 1990; *Hay et al.*, 2002; *Molnar*, 2004; *Willett*, 2010]. Such an explanation appears unlikely in the Greater Caucasus, however, for several reasons. First, the timing of increase in the rate of

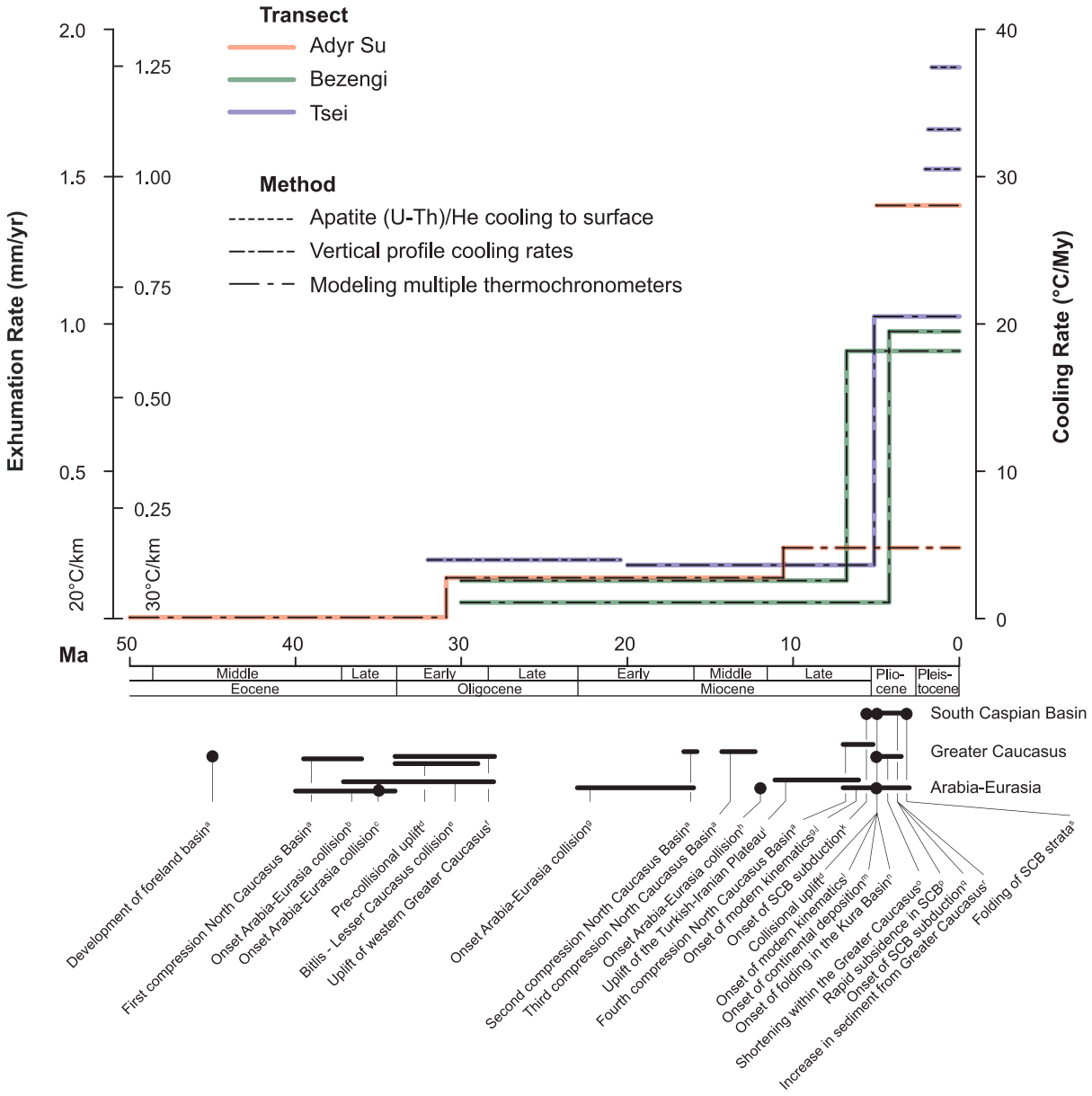

Figure 8. Summary of cooling rates from the central Greater Caucasus from a variety of methods (see Figures 4 and 6 and text for discussion) and comparison to regional tectonic events. Break points for changes in cooling rates, where observed, were determined from modeled cooling paths using piecewise linear regression. Cooling rates prior to 30 Ma are poorly constrained but indicate little to no cooling. All three transects exhibit cooling at ~4°C/Myr from 30 to 5 Ma and cooling at rates greater than ~20°/Myr since 5 Ma. Exhumation rates are given for geothermal gradients of 20°C/km and 30°C/km. Changes in cooling rates observed in the central Greater Caucasus are consistent with a latest Eocene or early Oligocene onset of collision along the Arabia-Eurasia boundary and appear to change in response to a latest Miocene or early Pliocene plate reorganization. Regional tectonic events are from the following sources: a, *Mikhailov et al.* [1999]; b, *Saintot and Angelier* [2002]; c, *Allen and Armstrong* [2008]; d, *Kral and Gurbanov* [1996]; e, *Şengör et al.* [2008]; f, *Vincent et al.* [2007]; g, *Allen et al.* [2004]; h, *McQuarrie et al.* [2003]; i, *Şengör et al.* [2003]; j, *Copley and Jackson* [2006]; k, *Allen et al.* [2002]; l, *Westaway* [1994]; m, *Khain* [1994]; n, *Forte et al.* [2010]; o, *Philip et al.* [1989]; p, *Brunet et al.* [2003]; q, *Jackson et al.* [2002]; r, *Morton et al.* [2003]; s, *Devlin et al.* [1999].

exhumation in the central Greater Caucasus is not observed elsewhere in the range [*Vincent et al.*, 2010]. Second, the end of the Miocene is marked by a switch from marine to nonmarine sedimentation in the eastern Greater Caucasus, reflecting topographic uplift [*Kopp and Shcherba*, 1985], and by a shift in sediment sources supplying the Caspian Sea from the Russian platform to the Greater Caucasus [*Morton et al.*, 2003]. Third, the structural evolution of the

Table A1. Single-Grain Apatite (U-Th)/He Replicate Data

Sample	Age[a] (Ma)	U (ppm)	Th (ppm)	^{4}He (nmol/g)	Mass (μg)	Ft[b]	r[c] (μm)	Sm (ppm)
T4	1.11 ± 0.04	1.44	3.69	0.02	17.05	0.64	40.0	1294.48
T4	2.38 ± 0.09	8.61	25.55	0.13	2.78	0.65	42.5	135.57
T4	1.82 ± 0.06	1.37	4.15	0.02	21.43	0.66	40.0	479.73
T4	1.44 ± 0.05	1.44	3.84	0.02	16.50	0.66	42.5	885.95
T4	1.61 ± 0.06	1.35	3.81	0.02	16.90	0.65	40.0	465.77
T3	3.74 ± 0.12	1.67	4.33	0.04	28.20	0.66	43.0	270.75
T3	1.58 ± 0.06	1.36	3.64	0.02	18.43	0.64	40.5	348.73
T3	1.20 ± 0.04	1.40	4.17	0.01	20.14	0.64	40.0	529.71
T3	0.98 ± 0.04	1.37	3.30	0.01	11.62	0.60	39.0	866.74
T2	2.79 ± 0.10	8.74	25.71	0.15	2.78	0.66	45.0	137.52
T2	0.71 ± 0.03	1.47	3.98	0.01	15.03	0.65	39.0	501.72
T2	1.32 ± 0.05	1.38	3.87	0.01	17.63	0.63	39.0	383.02
T2	1.82 ± 0.05	11.08	29.24	0.18	2.98	0.66	43.0	174.61
T2	3.63 ± 0.12	1.81	3.93	0.05	19.76	0.67	46.5	638.43
T1	2.06 ± 0.07	12.61	35.06	0.15	2.38	0.63	39.5	99.21
T1	3.28 ± 0.11	14.72	43.70	0.29	3.13	0.65	39.5	164.80
T1	2.43 ± 0.09	1.39	3.54	0.03	14.48	0.65	44.5	549.41
T1	4.37 ± 0.14	10.25	29.16	0.28	3.11	0.68	46.5	142.79
T1	1.31 ± 0.04	2.67	4.26	0.02	23.81	0.66	38.5	296.13
T1	1.83 ± 0.07	1.49	3.77	0.02	13.99	0.62	38.0	798.19
B3	14.6 ± 0.15	32.64	29.16	2.61	15.00	0.82	88.0	146.02
B3	9.50 ± 0.13	30.40	5.63	1.33	10.13	0.81	83.5	171.24
B3	13.11 ± 0.20	17.60	3.64	1.08	15.33	0.78	68.0	619.52
B3	11.38 ± 0.19	47.47	4.97	2.29	5.84	0.75	58.5	202.40
B2	3.98 ± 0.02	112.14	3.66	2.19	17.87	0.88	136.0	2008.81
B2	4.28 ± 0.03	77.45	3.46	1.58	12.82	0.84	93.5	1871.55
B2[d]	14.89 ± 0.10	91.69	3.80	6.55	13.31	0.85	105.0	1950.75
B2	4.94 ± 0.04	62.06	1.75	1.38	13.38	0.82	84.0	164.58
B2	3.03 ± 0.03	99.04	3.44	1.33	7.54	0.80	82.0	229.74
B6	8.46 ± 0.51	27.71	14.68	1.20	13.07	0.83	84.5	168.15
B6	20.00 ± 1.20	27.86	39.68	3.09	6.05	0.76	54.0	221.37
B6	13.09 ± 0.79	28.04	72.31	2.43	6.91	0.75	54.5	262.76
B6	12.65 ± 0.76	20.52	23.52	1.36	6.20	0.75	52.5	205.29
B5[d]	53.61 ± 3.22	106.70	1.78	26.74	11.20	0.85	117.5	200.93
B5	14.87 ± 0.89	63.12	2.94	3.73	2.48	0.72	45.0	108.79
B5	21.12 ± 1.27	192.63	11.62	16.59	2.33	0.74	52.0	198.66
B5	21.11 ± 1.27	67.65	1.87	5.90	3.09	0.75	53.0	168.97
B4	16.37 ± 0.98	37.36	20.13	2.77	5.24	0.74	48.0	116.43
B4	8.70 ± 0.52	27.55	16.21	1.07	2.55	0.72	46.5	90.80
B4	9.32 ± 0.56	29.68	22.46	1.31	3.21	0.73	47.5	122.61
B4	12.18 ± 0.73	23.79	22.54	1.39	4.41	0.71	44.5	131.70
B1	10.16 ± 0.61	89.16	39.93	4.11	3.45	0.75	54.0	378.47
B1	22.34 ± 1.34	87.20	39.37	8.78	3.07	0.74	52.0	370.05
B1	11.89 ± 0.71	83.06	42.99	4.89	7.58	0.81	73.0	229.81
B1	22.87 ± 1.37	92.31	33.96	9.89	6.47	0.79	62.5	286.95

[a]The 1σ errors are propagated from U, Th, and He measurement uncertainties.
[b]Alpha ejection correction of *Farley et al.* [1996].
[c]Grain radius.
[d]Tested positive as an outlier on the Q-test [*Dean and Dixon*, 1951] with 95% confidence when compared with other replicates from the same sample.

Greater Caucasus is opposite to that expected from climate-forced exhumation. Climate enhanced erosion acts on existing topographic barriers, removing gravitational loads, and thus localizing shortening on existing faults [e.g., *Wobus et al.*, 2003]. The Greater Caucasus, on the other hand, experience a region-wide propagation of deformation outward into surrounding foreland basins [e.g., *Forte et al.*, 2010], suggesting a tectonic, rather than climatic, force is driving the observed increase in exhumation rate.

[38] Finally, the increase in exhumation rate within the Greater Caucasus is coincident with a major plate boundary reorganization (Figure 8 [*Westaway*, 1994; *Allen et al.*, 2004; *Copley and Jackson*, 2006]). This reorganization has been suggested to result from deformation along the edges of thickened and shortened Turkish-Iranian Plateau

Table A2. Single-Grain Zircon (U-Th)/He Data

Sample	Age (Ma)	U (ppm)	Th (ppm)	He (nmol/g)	Mass (μg)	Ft	r (μm)
B1	188.50 ± 3.87	714.94	147.81	576.8	4.46	0.75	39.5
A1	24.06 ± 0.49	2095.89	101.64	207.01	4.13	0.75	39.8
A2	88.93 ± 1.81	673.17	68.66	240.11	2.88	0.72	34.8
T3	32.04 ± 0.72	655.24	418.65	95.07	4.9	0.73	33.8
T1	20.40 ± 0.39	679.60	448.29	64.89	4.48	0.75	39.5

Table A3. Apatite and Zircon Fission Track Data[a]

Sample	Grains (dmnls)	Dpar (μm)	Dper (μm)	N_s (tracks)	Area Analyzed ($cm^2 \times 10^{-3}$)	$\Sigma(P\Omega) \pm 1\sigma$ ($cm^2 \times 10^{-4}$)	$\xi_{MS} \pm 1\sigma$	$^{43}Ca(ap):^{29}Si(zr)$ (bkg:sig) ($\times 10^{-2}$) (dmnls)	^{238}U (bkg:sig) ($\times 10^{-2}$) (dmnls)	Q	Pooled Age (Ma)	Mean Length (μm)
						Apatite[b]						
A1	25	1.35	0.3	88	1.16	1.42 ± 0.0448	16.61 ± 0.42	3.67	1.23	0.82	5.16 ± 0.59	13.63 ± 1.86
A2	20	1.36	0.27	94	0.754	1.53 ± 0.0362	16.56 ± 0.42	3.37	2.80	0.15	5.09 ± 0.55	12.37 ± 1.67
B1	25	1.31	0.22	702	1.17	2.68 ± 0.0558	16.65 ± 0.42	3.49	6.06	0	21.8 ± 1.1	12.63 ± 2.07
B2	25	1.29	0.28	119	1.18	2.57 ± 0.0456	15.75 ± 0.39	4.79	31.3	0.13	3.64 ± 0.35	13.74 ± 1.64
B3	24	1.33	0.25	278	0.949	2.90 ± 0.0548	15.97 ± 0.39	2.92	0.516	0.07	7.64 ± 0.52	13.82 ± 1.73
T1	24	1.35	0.35	42	0.655	0.545 ± 0.0122	16.19 ± 0.39	6.41	19.7	0.02	6.23 ± 0.98	13.9 ± 1.7
						Zircon[c]						
A1	10			464	0.0301	0.091 ± 0.00044	9.22 ± 0.3	11.3	3.04	0	230 ± 13	
B1	20			1410	0.0890	0.207 ± 0.00072	8.81 ± 0.29	12.2	6.01	0	293 ± 12	

[a]Here dmnls, dimensionless; bkg:sig, background:signal.
[b]Analyst is Paul O'Sullivan, Apatite to Zircon, Inc.
[c]Analyst is Ray Donelick, Apatite to Zircon, Inc.

and Greater Caucasus crust [*Allen et al.*, 2004]. As noted above, it seems improbable that the Greater Caucasus were a highstanding mountain range prior to the time of this reorganization. Thus, the uplift of the Turkish-Iranian plateau alone would have to be interpreted as the driving force of the post-Miocene reorganization of the plate boundary, including the uplift in the Greater Caucasus. Alternatively, reorganization of the Arabia-Eurasia orogen could be driven by the final closure of the Greater Caucasus back-arc basin in late Miocene time. Such a closure would result in the cessation of subduction of oceanic or transitional crust across much of the Arabia-Eurasia collision zone, and thus mark the onset of throughgoing "hard" continent-continent collision, from the Arabian shield to the Scythian platform. Given a relatively steady rate of Arabia-Eurasia convergence [*McQuarrie et al.*, 2003], the disappearance of the last subduction zone would result in increased tectonic stresses throughout the orogen, resulting in plate boundary reorganization, including the initiation of Anatolian extrusion [*Allen et al.*, 2004] and orogenesis in previously slowly

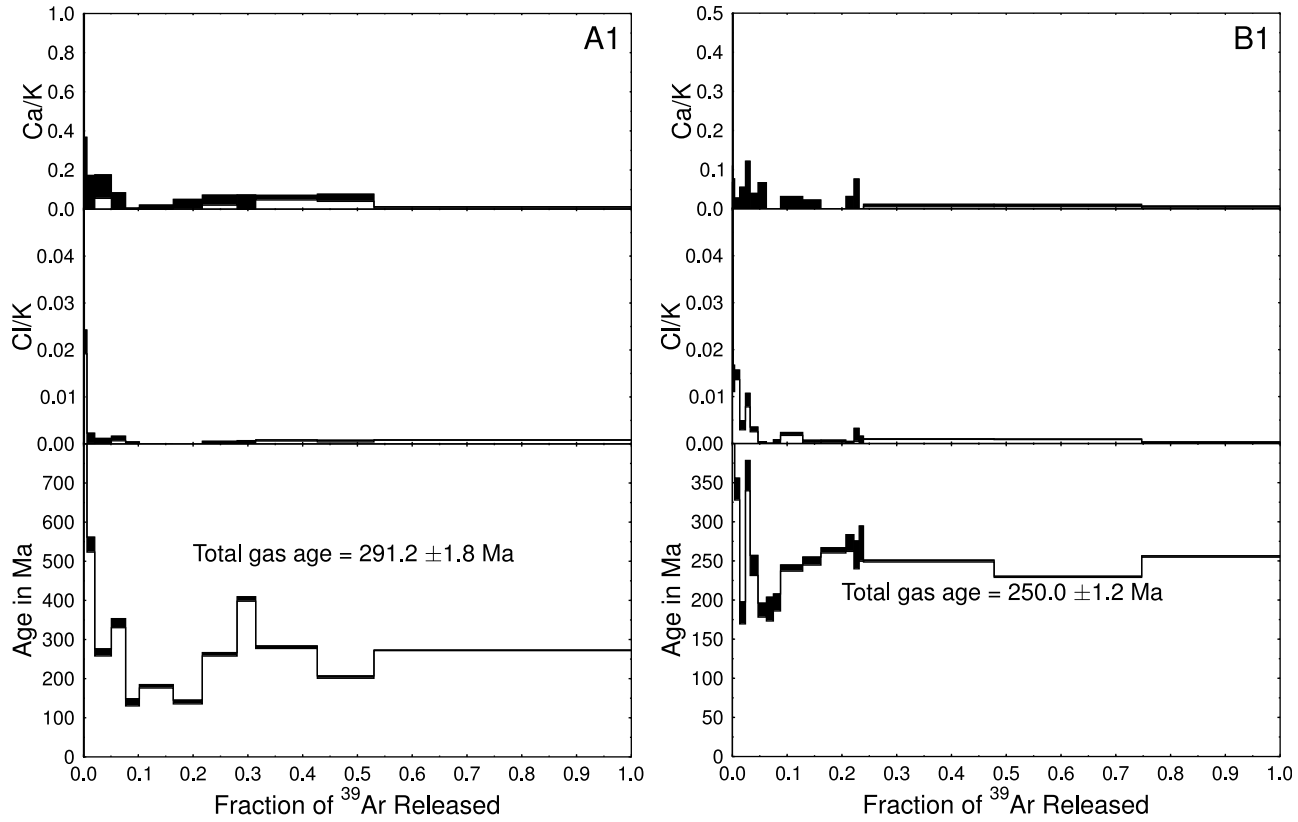

Figure A1. K-feldspar $^{40}Ar/^{39}Ar$ data.

deforming regions such as the Alborz [*Axen et al.*, 2001] and Greater Caucasus.

5. Conclusions

[39] Exhumation of the central Greater Caucasus occurred in two phases, beginning in Oligocene time. During the first phase, cooling rates increased from negligible values to ~4°C/Myr, likely in response to the collision of Arabia with the Pontide–Lesser Caucasus arc. Cooling rates remained constant throughout the late Oligocene and Miocene until ~5 Ma, when they rapidly increased to 20°C/Myr or more. This change coincides with a major plate boundary reorganization, as well as the onset of global climatic cooling. A variety of evidence suggests that rapid Pliocene exhumation of the central Greater Caucasus is tectonically driven, and we interpret this exhumation as resulting from either the closure of the Greater Caucasus basin and the onset of continent-continent collision across the Arabia-Eurasia plate boundary, or the migration of deformation away from the uplifted Turkish-Iranian plateau. If the former hypothesis is correct, then the post-Miocene reorganization is likely a result of the onset of "hard" continent-continent collision in this segment of the Arabia-Eurasia orogen.

Appendix A

[40] This section includes data for single-grain apatite (Table A1) and zircon (Table A2) (U-Th)/He concentrations, fission track counts (Table A3), and feldspar argon release spectra (Figure A1), along with corresponding age estimates.

[41] **Acknowledgments.** Ken Farley, Pete Reiners, Chris Hall, Ray Donelick, and Paul O'Sullivan are thanked for assistance with thermochronometric analyses. Discussions with Eric Cowgill, Ibrahim Murtuzayev, and Adam Forte were valuable in improving our understanding of the geology of the Caucasus region. Andrei Khudolei provided assistance in obtaining geological maps of Russia. This work was funded by Civilian Research and Development Fund (AZG1-2840-BA-06) and National Science Foundation (EAR-0810067) grants to N.A.N. and a Rackham International Student Fellowship from the University of Michigan to B.A. Charles Verdel and Stephen Vincent provided comments on an earlier version of the manuscript. Finally, we thank an anonymous reviewer and Gary Axen for their thoughtful reviews.

References

Alavi, M. (1994), Tectonics of the zagros orogenic belt of Iran: New data and interpretations, *Tectonophysics*, *229*(3–4), 211–238.

Allen, M. B., and H. A. Armstrong (2008), Arabia-Eurasia collision and the forcing of mid-Cenozoic global cooling, *Palaeogeogr. Palaeoclimatol. Palaeoecol.*, *265*(1–2), 52–58, doi:10.1016/j.palaeo.2008.04.021.

Allen, M. B., S. Jones, A. Ismail-Zadeh, M. Simmons, and L. Anderson (2002), Onset of subduction as the cause of rapid Pliocene-Quaternary subsidence in the South Caspian basin, *Geology*, *30*(9), 775–778.

Allen, M., J. Jackson, and R. Walker (2004), Late Cenozoic reorganization of the Arabia-Eurasia collision and the comparison of short-term and long-term deformation rates, *Tectonics*, *23*, TC2008, doi:10.1029/2003TC001530.

Arpat, E., and F. Şaroğlu (1972), The East Anatolian fault system: Thoughts on its development, *Bull. Miner. Res. Explor. Inst. Turk.*, *78*, 33–39.

Axen, G. J., P. S. Lam, M. Grove, D. F. Stockli, and J. Hassanzadeh (2001), Exhumation of the west-central Alborz Mountains, Iran, Caspian subsidence, and collision-related tectonics, *Geology*, *29*(6), 559–562.

Banks, C. J., A. G. Robinson, and M. P. Williams (1997), Structure and regional tectonics of the Achara-Trialet fold belt and the adjacent Rioni and Kartli foreland basins, Republic of Georgia: Regional and petroleum geology of the Black Sea and surrounding region, *AAPG Mem.*, *68*, 331–345.

Blythe, A. E., D. W. Burbank, A. Carter, K. Schmidt, and J. Putkonen (2007), Plio-Quaternary exhumation history of the central Nepalese Himalaya: 1. Apatite and zircon fission track and apatite [U-Th]/He analyses, *Tectonics*, *26*, TC3002, doi:10.1029/2006TC001990.

Boztuğ, D., and R. C. Jonckheere (2007), Apatite fission track data from central Anatolian granitoids (Turkey): Constraints on Neo-Tethyan closure, *Tectonics*, *26*, TC3011, doi:10.1029/2006TC001988.

Braun, J. (2003), Pecube: A new finite-element code to solve the 3D heat transport equation including the effects of a time-varying, finite amplitude surface topography, *Comput. Geosci.*, *29*(6), 787–794, doi:10.1016/S0098-3004(03)00052-9.

Braun, J. (2005), Quantitative constraints on the rate of landform evolution derived from low-temperature thermochronology, in *Low-Temperature Thermochronology: Techniques, Interpretations, and Applications*, edited by P. W. Reiners and T. A. Ehlers, *Rev. Mineral. Geochem.*, *58*, 351–374.

Brunet, M.-F., M. V. Korotaev, A. V. Ershov, and A. M. Nikishin (2003), The South Caspian Basin: A review of its evolution from subsidence modelling, *Sediment. Geol.*, *156*, 119–148.

Burbank, D. W. (2002), Rates of erosion and their implications for exhumation, *Mineral. Mag.*, *66*, 25–52.

Clark, M. K., and R. Bilham (2008), Miocene rise of the Shillong Plateau and the beginning of the end for the eastern Himalaya, *Earth Planet. Sci. Lett.*, *269*(3–4), 336–350.

Cloetingh, S., et al. (2007), TOPO-EUROPE: The geoscience of coupled deep Earth-surface processes, *Global Planet. Change*, *58*(1–4), 1–118, doi:10.1016/j.gloplacha.2007.02.008.

Copley, A., and J. Jackson (2006), Active tectonics of the Turkish-Iranian plateau, *Tectonics*, *25*, TC6006, doi:10.1029/2005TC001906.

Dean, R. B., and W. J. Dixon (1951), Simplified statistics for small numbers of observations, *Anal. Chem.*, *23*(4), 636–638.

Devlin, W. J., J. M. Cogswell, G. M. Gaskins, G. H. Isaksen, D. M. Pitcher, D. P. Puls, K. O. Stanley, and G. R. T. Wall (1999), South Caspian basin: young, cool, and full of promise, *GSA Today*, *9*(7), 1–9.

Dewey, J. F., M. R. Hempton, W. S. F. Kidd, F. Şaroğlu, and A. M. C. Şengör (1986), Shortening of continental lithosphere: The neotectonics of eastern Anatolia, a young collision zone, in *Processes of Collision Orogeny*, edited by M. P. Coward and A. C. Ries, *Geol. Soc. Spec. Publ.*, *19*, 3–36.

Dodson, M. H. (1973), Closure temperature in cooling geochronological and petrological systems, *Contrib. Mineral. Petrol.*, *40*(3), 259–274.

Donelick, R. A., P. B. O'Sullivan, and R. A. Ketcham (2005), Apatite fission-track analysis, in *Low-Temperature Thermochronology: Techniques, Interpretations, and Applications*, edited by P. W. Reiners and T. A. Ehlers, *Rev. Mineral. Geochem.*, *58*, 49–94.

Donnelly, T. W. (1982), Worldwide continental denudation and climatic deterioration during the late tertiary—Evidence from deep-sea sediments, *Geology*, *10*(9), 451–454.

Ehlers, T. A., et al. (2005), Computational tools for low-temperature thermochronometer interpretation, in *Low-Temperature Thermochronology: Techniques, Interpretations, and Applications*, edited by P. W. Reiners and T. A. Ehlers, *Rev. Mineral. Geochem.*, *58*, 589–622.

England, P., and P. Molnar (1990), Surface uplift, uplift of rocks, and exhuamtion of rocks, *Geology*, *18*(12), 1173–1177.

Ershov, A. V., M.-F. Brunet, A. M. Nikishin, S. N. Bolotov, B. P. Nazarevich, and M. V. Korotaev (2003), Northern Caucasus basin: Thermal history and synthesis of subsidence models, *Sediment. Geol.*, *156*, 95–118.

Fakhari, M. D., G. J. Axen, B. K. Horton, J. Hassanzadeh, and A. Amini (2008), Revised age of proximal deposits in the Zagros foreland basin and implications for Cenozoic evolution of the High Zagros, *Tectonophysics*, *451*(1–4), 170–185, doi:10.1016/j.tecto.2007.11.064.

Fakhari, M. D., B. Guest, G. Axen, and B. K. Horton (2009), Evidence for significant dextral faulting within the High Zagros, Iran, *Abstr. Programs*, *41*, 406.

Farley, K. A. (2000), Helium diffusion from apatite: General behavior as illustrated by Durango fluorapatite, *J. Geophys. Res.*, *105*, 2903–2914, doi:10.1029/1999JB900348.

Farley, K. A. (2002), (U-Th)/He dating: Techniques, calibrations, and applications, in *Noble Gases in Geochemistry and Cosmochemistry*, edited by D. Porcelli, C. J. Ballentine, and R. Wieler, *Rev. Mineral. Geochem.*, *47*, 819–844.

Farley, K. A., and D. F. Stockli (2002), (U-Th)/He dating of phosphates: Apatite, monazite, and xenotime, in *Phosphates: Geochemical, Geobiological, and Materials Importance*, edited by M. Kohn, J. Rakovan, and J. Hughes, *Rev. Mineral. Geochem.*, *48*, 559–577.

Farley, K. A., R. A. Wolf, and L. T. Silver (1996), The effects of long alpha-stopping distances on (U-Th)/He ages, *Geochim. Cosmochim. Acta*, *60*(21), 4223–4229.

Flowers, R. M., R. A. Ketcham, D. L. Shuster, and K. A. Farley (2009), Apatite (U-Th)/He thermochronometry using a radiation damage accu-

mulation and annealing model, *Geochim. Cosmochim. Acta*, *73*(8), 2347–2365, doi:10.1016/j.gca.2009.01.015.
Foland, K. A. (1994), Argon diffusion in feldspars, in *Feldspars and Their Reactions*, edited by I. Parsons, *NATO ASI Ser., Ser. C*, *421*, 415–447.
Forte, A., E. Cowgill, T. Bernardin, O. Kreylos, and B. Hamann (2010), Late Cenozoic deformation of the Kura fold-thrust belt, southern Greater Caucasus, *Geol. Soc. Am. Bull.*, *122*(3–4), 465–486.
Gallagher, K., J. Stephenson, R. Brown, C. Holmes, and P. Fitzgerald (2005), Low temperature thermochronology and modeling strategies for multiple samples 1: Vertical profiles, *Earth Planet. Sci. Lett.*, *237*(1–2), 193–208, doi:10.1016/j.epsl.2005.06.025.
Gamkrelidze, P. D., and I. R. Kakhadze (1959), Caucasus series K-38-VII, geological map, scale 1:200,000, Russ. Geol. Res. Inst., St. Petersburg, Russia.
Gleadow, A. J. W., I. R. Duddy, J. F. Lovering, and B. R. Griffith (1983), Fission track analysis: A new tool for the evaluation of thermal histories and hydrocarbon potential—Developing for the future, *APEA J.*, *23*, 93–102.
Golonka, J. (2004), Plate tectonic evolution of the southern margin of Eurasia in the Mesozoic and Cenozoic, *Tectonophysics*, *381*(1–4), 235–273.
Guest, B., D. F. Stockli, M. Grove, G. J. Axen, P. S. Lam, and J. Hassanzadeh (2006), Thermal histories from the central Alborz mountains, northern Iran: Implications for the spatial and temporal distribution of deformation in northern Iran, *Geol. Soc. Am. Bull.*, *118*(11–12), 1507–1521, doi:10.1130/B25819.1.
Hasebe, N., J. Barbarand, K. Jarvis, A. Carter, and A. Hurford (2004), Apatite fission-track chronometry using laser ablation ICP-MS, *Chem. Geol.*, *207*(3–4), 135–145, doi:10.1016/j.chemgeo.2004.01.007.
Hay, W. W., E. Soeding, R. M. DeConto, and C. N. Wold (2002), The Late Cenozoic uplift—Climate change paradox, *Int. J. Earth Sci.*, *91* (5), 746–774, doi:10.1007/s00531-002-0263-1.
Hempton, M. (1987), Constraints on Arabian plate motion and extensional history of the Red Sea, *Tectonics*, *6*(6), 687–705.
House, M. A., K. A. Farley, and D. Stockli (2000), Helium chronometry of apatite and titanite using Nd-YAG laser heating, *Earth Planet. Sci. Lett.*, *183*(3–4), 365–368.
Jackson, J., K. Priestley, M. Allen, and M. Berberian (2002), Active tectonics of the South Caspian basin, *Geophys. J. Int.*, *148*(2), 214–245.
Jassim, S. Z., and J. C. Goff (2006), *Phanerozoic Development of the Northern Arabian Plate*, Geol. of Iraq, Dolin, Prague and Moravian Mus., Brno, Czech Republic.
Kadirov, F., S. Mammadov, R. Reilinger, and S. McClusky (2008), Some new data on modern tectonic deformation and active faulting in Azerbaijan (according to Global Positioning System measurements), *Proc. Sci. Earth Azerbaijan Natl. Acad. Sci.*, *1*, 82–88.
Kay, S. M., and B. L. Coira (2009), Shallowing and steepening subduction zones, continental lithospheric loss, magmatism, and crustal flow under the central Andean Altiplano-Puna Plateau, in *Backbone of the Americas: Shallow Subduction, Plateau Uplift, and Ridge and Terrane Collision*, edited by S. M. Kay, V. A. Ramos, and W. R. Dickinson, *Mem. Geol. Soc. Am.*, *204*, 229–259, doi:10.1130/2009.1204(11).
Ketcham, R. A. (2005), Forward and inverse modeling of low-temperature thermochronometry data, *Rev. Mineral. Geochem.*, *58*, 275–314, doi:10.2138/rmg.2005.58.11.
Ketcham, R. A., A. Carter, R. A. Donelick, J. Barbarand, and A. J. Hurford (2007), Improved measurement of fission-track annealing in apatite using c-axis projection, *Am. Mineral.*, *92*(5–6), 789–798, doi:10.2138/am.2007.2280.
Ketcham, R. A., R. A. Donelick, M. L. Balestrieri, and M. Zattin (2009), Reproducibility of apatite fission-track length data and thermal history reconstruction, *Earth Planet. Sci. Lett.*, *284*(3–4), 504–515, doi:10.1016/j.epsl.2009.05.015.
Khain, E. V. (1994), Alpine belt of southern Ex-USSR, in *Geology of Northern Eurasia*, vol. 2, *Phanerozoic Fold Belts and Young Platforms*, chap. 5, *Beiträge Reg. Geol. Erde*, 17, 130–235.
Knapp, C. C., J. H. Knapp, and J. A. Connor (2004), Crustal-scale structure of the South Caspian Basin revealed by deep seismic reflection profiling, *Mar. Pet. Geol.*, *21*, 1073–1081.
Kopp, M. L. (2007), Late Alpine collision tectonics of the Caucasus, in *The Greater Caucasus During the Alpine Epoch*, edited by J. G. Leonov, pp. 285–316, Geos, Moscow.
Kopp, M. L., and I. G. Shcherba (1985), Late Alpine development of the east Caucasus, *Geotectonics*, *19*(6), 497–507.
Kral, J., and A. Gurbanov (1996), Apatite fission track data from the Great Caucasus pre-Alpine basement, *Chem. Erde*, *56*, 177–192.
Leonov, M. (2007), Tectonic-gravitational mixtites of the central segment of southern slope of the Greater Caucasus, in *The Greater Caucasus During the Alpine Epoch*, edited by J. G. Leonov, pp. 231–250, Geos, Moscow.
McAleer, R. J., J. A. Spotila, E. Enkelmann, and A. L. Berger (2009), Exhumation along the Fairweather fault, southeastern Alaska, based on low-temperature thermochronometry, *Tectonics*, *28*, TC1007, doi:10.1029/2007TC002240.
McDowell, F. W., W. C. McIntosh, and K. A. Farley (2005), A precise $^{40}Ar/^{39}Ar$ reference age for the Durango apatite (U-Th)/He and fission-track dating standard, *Chem. Geol.*, *214*(3–4), 249–263.
McQuarrie, N., J. M. Stock, C. Verdel, and B. P. Wernicke (2003), Cenozoic evolution of Neotethys and implications for the causes of plate motions, *Geophys. Res. Lett.*, *30*(20), 2036, doi:10.1029/2003GL017992.
Mikhailov, V., L. Panina, R. Polino, N. Koronovsky, E. Kiseleva, N. Klavdieva, and E. Smolyaninova (1999), Evolution of the North Caucasus foredeep: Constraints based on the analysis of subsidence curves, *Tectonophysics*, *307*(3–4), 361–379.
Milanovsky, E. E., and V. E. Khain (1963), *Geological Structure of Caucasus*, Moscow State Univ., Moscow.
Mitchell, S. G., and P. W. Reiners (2003), Influence of wildfires on apatite and zircon (U-Th)/He ages, *Geology*, *31*(12), 1025–1028, doi:10.1130/G19758.1.
Molnar, P. (2004), Late Cenozoic increase in accumulation rates of terrestrial sediment: How might climate change have affected erosion rates?, *Annu. Rev. Earth Planet. Sci.*, *32*, 67–89, doi:10.1146/annurev.earth.32.091003.143456.
Molnar, P., and P. England (1990), Late Cenozoic uplift of mountain ranges and global climate change—Chicken or egg?, *Nature*, *346*(6279), 29–34.
Morton, A., M. Allen, M. Simmons, F. Spathopoulos, J. Still, D. Hinds, A. Ismail-Zadeh, and S. Kroonenberg (2003), Provenance patterns in a neotectonic basin: Pliocene and Quaternary sediment supply to the South Caspian, *Basin Res.*, *15*(3), 321–337.
Nalivkin, D. V. (1976), *Geological Map of the USSR 1:500,000*, Russ. Geol. Res. Inst., St. Petersburg, Russia.
Nikishin, A. M., P. A. Ziegler, D. I. Panov, B. P. Nazarevich, M.-F. Brunet, R. A. Stephenson, S. N. Bolotov, M. V. Korotaev, and P. L. Tikhomirov (2001), Mesozoic and Cainozoic evolution of the Scythian platform–Black sea–Caucasus domain, in *Peri-Tethys Memoir 6: Peri-Tethyan Rift/Wrench Basins and Passive Margins*, edited by P. Ziegler et al., *Mem. Mus. Natl. Hist. Nat.*, *186*, 295–346.
Okay, A. I., M. Zattin, and W. Cavazza (2010), Apatite fission-track data for the Miocene Arabia-Eurasia collision, *Geology*, *38*(1), 35–38, doi:10.1130/G30234.1.
Ownby, S., H. D. Granados, R. A. Lange, and C. M. Hall (2007), Volcán Tancítaro, Michoacín, Mexico, $^{40}Ar/^{39}Ar$ constraints on its history of sector collapse, *J. Volcanol. Geotherm. Res.*, *161*(1–2), 1–14, doi:10.1016/j.jvolgeores.2006.10.009.
Philip, H., A. Cisternas, A. Gvishiani, and A. Gorshkov (1989), The Caucasus: An actual example of the initial stages of continental collision, *Tectonophysics*, *161*(1–2), 1–21.
Philippot, P., J. Blichert-Toft, A. Perchuk, S. Costa, and V. Gerasimov (2001), Lu-Hf and Ar-Ar chronometry supports extreme rate of subduction zone metamorphism deduced from geospeedometry, *Tectonophysics*, *342*(1–2), 23–38, doi:10.1016/S0040-1951(01)00155-X.
Pindell, J., L. Kennan, W. V. Maresch, K.-P. Stanek, G. Drapper, and R. Higgs (2005), Plate-kinematics and crustal dynamics of circum-Caribbean arc-continent interactions: Tectonic controls on basin development in Proto-Caribbean margins, in *Caribbean-South American Plate Interactions, Venezuela*, edited by H. G. Avé Lallemant and V. B. Sisson, *Spec. Pap. Geol. Soc. Am.*, *394*, 7–52.
Pismennyj, A. N. (2002), Caucasus series K-38VIII,XIV, in *Russian State Geological Map*, 2nd ed., scale 1:200,000, Russ. Geol. Res. Inst., St. Petersburg, Russia.
Reilinger, R., et al. (2006), GPS constraints on continental deformation in the Africa-Arabia-Eurasia continental collision zone and implications for the dynamics of plate interactions, *J. Geophys. Res.*, *111*, B05411, doi:10.1029/2005JB004051.
Reiners, P. W., and M. T. Brandon (2006), Using thermochronology to understand orogenic erosion, *Annu. Rev. Earth Planet. Sci.*, *34*, 419–466, doi:10.1146/annurev.earth.34.031405.125202.
Reiners, P. W., K. A. Farley, and H. J. Hickes (2002), He diffusion and (U-Th)/He thermochronometry of zircon: Initial results from Fish Canyon Tuff and Gold Butte, *Tectonophysics*, *349*(1–4), 297–308, doi:10. 1016/S0040-1951(02)00058-6.
Reiners, P. W., T. A. Ehlers, S. G. Mitchell, and D. R. Montgomery (2003), Coupled spatial variations in precipitation and long-term erosion rates across the Washington Cascades, *Nature*, *426*(6967), 645–647.
Reiners, P. W., T. L. Spell, S. Nicolescu, and K. A. Zanetti (2004), Zircon (U-Th)/He thermochronometry: He diffusion and comparisons with

^{40}Ar/^{39}Ar dating, *Geochim. Cosmochim. Acta*, *68*(8), 1857–1887, doi:10.1016/j.gca.2003.10.021.

Robertson, A. H. F. (2000), Mesozoic-Tertiary tectonic-sedimentary evolution of a south Tethyan oceanic basin and its margins in southern Turkey: Tectonics and magmatism in Turkey and the surrounding area, *Geol. Soc. Spec. Publ.*, *173*, 97–138.

Robinson, A. G., J. H. Rudat, C. J. Banks, and R. L. F. Wiles (1996), Petroleum geology of the Black Sea, *Mar. Pet. Geol.*, *13*, 195–223.

Saintot, A., and J. Angelier (2002), Tectonic paleostress fields and structural evolution of the NW-Caucasus fold-and-thrust belt from Late Cretaceous to Quaternary, *Tectonophysics*, *357*(1–4), 1–31, doi:10.1016/S0040-1951(02)00360-8.

Saintot, A., M.-F. Brunet, F. Yakovlev, M. Sébrier, R. A. Stephenson, A. Ershov, F. Chalot-Prat, and T. McCann (2006), The Mesozoic-Cenozoic tectonic evolution of the Greater Caucasus, in *European Lithosphere Dynamics*, edited by D. G. Gee and R. A. Stephenson, *Geol. Soc. Mem.*, *32*, 277–289.

Samson, S. D., and E. C. Alexander (1987), Calibration of the interlaboratory ^{40}Ar-^{39}Ar dating standard, MMhb-1, *Chem. Geol.*, *66*(1–2), 27–34, doi:10.1016/0168-9622(87)90025-X.

Şengör, A. M. C., and W. S. F. Kidd (1979), Post-collisional tectonics of the Turkish-Iranian plateau and a comparison with Tibet, *Tectonophysics*, *55*(3–4), 361–376.

Şengör, A. M. C., S. Özeren, T. Genç, and E. Zor (2003), East Anatolian high plateau as a mantle-supported, north–south shortened domal structure, *Geophys. Res. Lett.*, *30*(24), 8045, doi:10.1029/2003GL017858.

Şengör, A. M. C., M. S. Özeren, M. Keskin, M. Sakinç, A. D. Özbakir, and İ. Kayan (2008), Eastern Turkish high plateau as a small Turkic-type orogen: Implications for post-collisional crust-forming processes in Turkic-type orogens, *Earth Sci. Rev.*, *90*(1–2), 1–48, doi:10.1016/j.earscirev.2008.05.002.

Shuster, D. L., and K. A. Farley (2009), The influence of artificial radiation damage and thermal annealing on helium diffusion kinetics in apatite, *Geochim. Cosmochim. Acta*, *73*(1), 183–196, doi:10.1016/j.gca.2008.10.013.

Shuster, D. L., R. M. Flowers, and K. A. Farley (2006), The influence of natural radiation damage on helium diffusion kinetics in apatite, *Earth Planet. Sci. Lett.*, *249*(3–4), 148–161, doi:10.1016/j.epsl.2006.07.028.

Somin, M. L. (2007a), Main features of structure of pre-Alpine basement of the Greater Caucasus, in *The Greater Caucasus During the Alpine Epoch*, edited by J. G. Leonov, pp. 15–38, Geos, Moscow.

Somin, M. L. (2007b), Alpine deformation of basement complexes and tectonic style of the Greater Caucasus, in *The Greater Caucasus During the Alpine Epoch*, edited by J. G. Leonov, pp. 111–140, Geos, Moscow.

Stocklin, J. (1974), Possible ancient continental margins in Iran, in *The Geology of Continental Margins*, edited by C. A. Burk and C. L. Drake, pp. 873–887, Springer, New York.

Tagami, T., R. F. Galbraith, R. Yamada, and G. M. Laslett (1998), Revised annealing kinetics of fission tracks in zircon and geological implications, in *Advances in Fission-Track Geochronology: International Workshop on Fission-Track Dating, Ghent, Belgium, 1996*, vol. 10, *Solid Earth Sci. Libr.*, edited by P. Van den Haute and F. De Corte, pp. 99–112, Kluwer Acad., Dordrecht, Netherlands.

Vincent, S. J., A. C. Morton, A. Carter, S. Gibbs, and T. G. Barabadze (2007), Oligocene uplift of the western Greater Caucasus: An effect of initial Arabia-Eurasia collision, *Terra Nova*, *19*(2), 160–166, doi:10.1111/j.1365-3121.2007.00731.x.

Vincent, S. J., A. Carter, V. A. Lavrishchev, S. P. Price, T. G. Barabadze, and N. Hovius (2010), The exhumation of the western Greater Caucasus: A thermochronometric study, *Geol. Mag.*, *148*(1), 1–21, doi:10.1017/S0016756810000257.

Wagner, G. A., and G. M. Reimer (1972), Fission track tectonics: The tectonic interpretation of fission track apatite ages, *Earth Planet. Sci. Lett.*, *14*(2), 263–268.

Wells, A. J. (1969), The crush zone of the Iranian Zagros mountains, and its implications, *Geol. Mag.*, *106*(5), 385–394.

Westaway, R. (1994), Present-day kinematics of the Middle-East and eastern Mediterranean, *J. Geophys. Res.*, *99*, 12,071–12,090.

Whipple, K., and G. Tucker (1999), Dynamics of the stream-power river incision model: Implications for height limits of mountain ranges, landscape response timescales, and research needs, *J. Geophys. Res.*, *104*, 17,661–17,674.

Willett, S. D. (2010), Late Neogene erosion of the alps: A climate driver?, *Annu. Rev. Earth Planet. Sci.*, *38*(1), 411–437, doi:10.1146/annurev-earth-040809-152543.

Wobus, C. W., K. V. Hodges, and K. X. Whipple (2003), Has focused denudation sustained active thrusting at the Himalayan topographic front?, *Geology*, *31*(10), 861–864, doi:10.1130/G19730.1.

Wolf, R., K. Farley, and L. Silver (1996), Helium diffusion and low-temperature thermochronometry of apatite, *Geochim. Cosmochim. Acta*, *60*(21), 4231–4240.

Yilmaz, Y. (1993), New evidence and model on the evolution of the southeast Anatolian orogen, *Geol. Soc. Am. Bull*, *105*(2), 251–271.

Zonenshain, L. P., and X. Le Pichon (1986), Deep basins of the Black Sea and Caspian Sea as remnants of Mesozoic back-arc basins, *Tectonophysics*, *123*(1–4), 181–211.

B. Avdeev and N. A. Niemi, Department of Geological Sciences, University of Michigan, 2534 C. C. Little Bldg., 1100 N. University Ave., Ann Arbor, MI 48109, USA. (borya@umich.edu; naniemi@umich.edu)